Does the Arctic Stratospheric Polar Vortex Exhibit Signs of Preconditioning Prior to Sudden Stratospheric Warmings?

ZACHARY D. LAWRENCE[a]

New Mexico Institute of Mining and Technology, Socorro, New Mexico

GLORIA L. MANNEY[b]

NorthWest Research Associates, Socorro, New Mexico

(Manuscript received 21 June 2019, in final form 25 September 2019)

ABSTRACT

Characteristics of the Arctic stratospheric polar vortex are examined using reanalysis data with dynamic time warping (DTW) and a clustering technique to determine whether the polar vortex exhibits canonical signs of preconditioning prior to sudden stratospheric warmings (SSWs). The DTW and clustering technique is used to locate time series motifs in vortex area, vortex edge-averaged PV gradients, and vortex edge-averaged wind speeds. Composites of the motifs reveal that prior to roughly 75% of SSWs, in the middle to upper stratosphere, PV gradients and wind speeds in the vortex edge region increase, and vortex area decreases. These signs agree with prior studies that discuss potential signals of preconditioning of the vortex. However, similar motifs are also found in a majority of years without SSWs. While such non-SSW motifs are strongly associated with minor warming signals apparent only in the middle and upper stratosphere, only roughly half of these can be associated with later "significant disturbances" (SDs) that do not quite meet the threshold for major SSWs. The median lead time for sharpening vortex edge PV gradients represented in the motifs prior to SSWs and SDs is ~25 days, while the median lead time for the vortex area and edge wind speeds is ~10 days. Overall, canonical signs of preconditioning do appear to exist prior to SSWs, but their existence in years without SSWs implies that preconditioning of the vortex may be an insufficient condition for the occurrence of SSWs.

1. Introduction

Sudden stratospheric warmings (SSWs) are some of the most extreme dynamical events that occur in Earth's atmosphere. As McIntyre (1982) put it, "[t]he stratospheric sudden warming is a large-scale experiment which nature kindly performs for us from time to time." Nearly 40 years later, with continuous monitoring of the atmosphere, we now know these "experiments" happen roughly 6 out of every 10 years, albeit with substantial decadal variability (e.g., Butler et al. 2017, and references therein). SSWs manifest as intense and abrupt disruptions of the westerly wintertime polar stratospheric circulation represented by the stratospheric polar vortex, accompanied by sudden increases in polar stratospheric temperatures. During such events the stratospheric polar vortex becomes highly distorted, either becoming displaced far off the pole or split apart into two or more "offspring" vortices (e.g., Charlton and Polvani 2007).

Many previous studies have shown that SSWs can exert a downward influence on the troposphere in ways that can influence regional seasonal weather and climate (e.g., Butler et al. 2014; Domeisen et al. 2015; Kidston et al. 2015; Charlton-Perez et al. 2018; Smith et al. 2018,

Denotes content that is immediately available upon publication as open access.

Supplemental information related to this paper is available at the Journals Online website: https://doi.org/10.1175/JAS-D-19-0168.s1.

[a] Current affiliation: Cooperative Institute for Research in Environmental Sciences, University of Colorado Boulder, and Physical Sciences Division, NOAA/Earth System Research Laboratory, Boulder, Colorado.

[b] Additional affiliation: Department of Physics, New Mexico Institute of Mining and Technology, Socorro, New Mexico.

Corresponding author: Zachary D. Lawrence, zachary.lawrence@noaa.gov

DOI: 10.1175/JAS-D-19-0168.1

and references therein). Although not all SSWs have appreciable tropospheric impacts (e.g., Karpechko et al. 2017), the occurrence of SSWs is often a boon for forecasting on subseasonal to seasonal time scales, as forecasts following SSWs tend to be more skillful (Sigmond et al. 2013; Scaife et al. 2016; Hansen et al. 2019).

While SSWs often lead to improved predictability in forecasts, predicting the SSWs themselves can be difficult. Given that SSWs can influence the tropospheric state, better predictability of SSWs could improve long-range forecasts (e.g., Sigmond et al. 2013; Tripathi et al. 2015; Scaife et al. 2016). Studies incorporating some of the most recent forecast models show that SSWs can usually be forecast 10–12 days in advance, though this varies across models and events (e.g., Tripathi et al. 2015, 2016; Karpechko 2018; Karpechko et al. 2018; Rao et al. 2018; Taguchi 2018, and references therein). This predictability range of roughly two weeks has been referred to as the ''deterministic limit'' for SSWs; useful predictability beyond the deterministic limit for SSWs can be achieved using probabilistic risk from ensembles of forecasts (e.g., Scaife et al. 2016) and statistical models that base predictions on dynamical variables (e.g., Kretschmer et al. 2017; Jucker and Reichler 2018). Forecasts and idealized model experiments of SSWs can be sensitive to many factors, including synoptic tropospheric systems and the position and strength of tropospheric blocking (e.g., Mukougawa et al. 2005; Nishii and Nakamura 2010; Karpechko et al. 2018), surface topography and tropospheric heating (e.g., Gerber and Polvani 2009; Sheshadri et al. 2015; White et al. 2018; Lindgren et al. 2018), vortex geometry (Taguchi 2016), and the stratospheric state itself (e.g., Hitchcock and Haynes 2016; Noguchi et al. 2016; de la Cámara et al. 2017; Martineau et al. 2018a).

Leveraging the stratospheric state remains an interesting avenue for improving predictability of SSWs. The triggering of an SSW implies a rapid and nearly simultaneous growth of wave fluxes throughout the stratosphere. Typically, this has been attributed to anomalous vertical wave fluxes supplied by the troposphere disturbing the stratospheric circulation (Matsuno 1971); such wave fluxes are often attributed to tropospheric precursor and blocking patterns (e.g., Martius et al. 2009; Cohen and Jones 2011; Bancalá et al. 2012; Díaz-Durán et al. 2017; Huang et al. 2018). However, nonlinear wave–mean flow feedbacks (e.g., Sjoberg and Birner 2014) and/or resonance behavior (e.g., Plumb 1981; Esler and Matthewman 2011; Matthewman and Esler 2011) can also generate realistic ''explosive'' growth of wave amplitudes; from these perspectives, the large amplification of wave activity is more a manifestation of SSWs rather than the cause. These ideas are not necessarily mutually exclusive nor intended to exclusively explain all SSWs (e.g., Birner and Albers 2017).

The polar wintertime stratosphere has commonly been said to be ''preconditioned'' when it is in a state that supports triggering an SSW, and thus ''preconditioning'' is the sum of all processes that coax the circulation into a preconditioned state (e.g., Albers and Birner 2014). Smith (1992) attempted to classify preconditioned initial conditions prior to SSWs, and found that such cases were independent of lower-boundary wave forcings, but sensitive to initial conditions within the stratosphere. A more recent study by de la Cámara et al. (2017) used targeted experiments with prescribed tropospheric evolution but a free running stratosphere and found that differences in the stratospheric state (preconditioning) could significantly alter the development toward or away from both split and displacement SSWs. The precise meaning of preconditioning differs based on whether the SSW-triggering mechanism in question relates to wave focusing or resonant excitation, but the inferred signatures of preconditioning are remarkably similar.

Early studies recognized that major warmings were often preceded by wave-1 minor warming–like disturbances in the middle and upper stratosphere (Kanzawa 1980; Labitzke 1981; Palmer 1981; Palmer and Hsu 1983). The importance of these precursor disturbances was highlighted by McIntyre (1982), who discussed how preconditioning could be interpreted as processes that focus wave activity into the polar vortex by sharpening the gradients of potential vorticity (PV) along the vortex edge. This edge sharpening is achieved by wave breaking events (such as those brought about by the aforementioned wave-1 precursors) that irreversibly mix the vortex high-PV and ''surf zone'' low-PV air (McIntyre and Palmer 1984), which can further change the shape and size of the vortex. Preconditioned states were sometimes discussed from a zonal-mean perspective via the quasigeostrophic refractive index to highlight when planetary waves could be preferentially guided into the polar region (e.g., Butchart et al. 1982; Lin 1982; O'Neill and Youngblut 1982; Palmer and Hsu 1983). Lin (1982) noted that a northward shift of the stratospheric jet seems to be favorable for the development of SSWs, which is a signal that has been shown to be apparent in lagged composites in the weeks prior to SSWs (Limpasuvan et al. 2004). The notion of edge sharpening discussed by McIntyre (1982) is consistent with changes to the latitudinal position of the stratospheric jet and the focusing of waves evidenced by the quasigeostrophic refractive index (see, e.g., the discussion in Albers and Birner 2014).

The process of edge sharpening reflects structural changes to the vortex. Robinson (1986) found that wave amplitudes in the stratosphere were sensitive to the size of the surf zone and vortex, such that the development of an SSW could be sensitive to rearrangements of PV induced by prior wave breaking. Baldwin and Holton (1988) demonstrated that the vortex was always reduced in size prior to the major warmings of the 1960s–80s. Scott et al. (2004) found that sharper PV gradients in lower levels of modeled vortices increased vertical wave propagation and wave breaking at upper levels. Kwasniok et al. (2019) noted that while mass stripping from the vortex is common prior to SSWs, there is no clear threshold of mass removed that seems related to triggering SSWs.

McIntyre (1982) also discussed the plausibility of resonance in triggering SSWs, particularly in light of early work on the subject (e.g., Clark 1974; Tung and Lindzen 1979; Plumb 1981). More recent modeling studies related to resonant excitation have more often considered the more barotropic vortex split SSWs (e.g., Matthewman and Esler 2011; Liu and Scott 2015; Scott 2016) as opposed to the baroclinic displacement SSWs (e.g., Esler and Matthewman 2011), but these have all noted the potential for preconditioning to be related to similar modifications to vortex structure and strength. For instance, Liu and Scott (2015) discussed how characteristics of preconditioning, such as reduced vortex area and increased vortex edge PV gradients, could correspond to changes in their model parameters that influence resonance. As Albers and Birner (2014) explain, in the context of resonance, preconditioning is better viewed as processes that modulate the vortex geometry and PV gradients toward the resonant excitation point.

O'Neill and Pope (1988) strongly questioned the notion of preconditioning based on wave–mean flow theory because of the prominence of nonlinear vortex–anticyclone interactions prior to and during SSWs. Sun et al. (2012) deemed tropospheric conditions as more important than stratospheric preconditioning, particularly in modeling experiments of wavenumber-1 forced displacement SSWs. Case studies of individual SSWs have often noted the importance of synoptic tropospheric systems associated with the development of SSWs (e.g., Coy et al. 2009; Coy and Pawson 2015; Attard et al. 2016). O'Neill et al. (2017) suggested a mechanism by which some vortex split SSWs arise from local tropospheric cyclogenesis underneath the tip of an elongated stratospheric vortex. Results like these illustrate the importance of nonlinear processes and localized tropospheric systems in the precise development of SSWs. However, in some cases these processes could be considered "preconditioners" [as noted, for instance, in Attard et al. (2016)].

While the notion of preconditioning itself depends on the SSW triggering mechanism, there may be mechanisms involved that are common to both. For instance, Domeisen et al. (2018) suggests that the phase speed of traveling waves may play an important role in preconditioning the stratosphere, regardless of the SSW triggering mechanism. The preceding discussion also suggests that studies have noted common symptoms of preconditioning regardless of the triggering mechanism, specifically those related to the size and strength of the vortex, and the PV gradients. Recently, Jucker and Reichler (2018) showed that meridional PV gradients in the stratosphere were useful for statistical prediction of SSWs beyond the deterministic limit.

The aim of this study is to seek out supposed symptoms of preconditioning prior to SSWs primarily from the perspective of the vortex itself rather than the zonal-mean circulation or quantities based on it. Studies based on composites relative to the onsets of SSWs are relatively common. However, compositing relative to SSW events themselves presupposes that processes occurring before these events happen at roughly the same times and across the same time scales, since otherwise the signals would not be strongly apparent in the composites. Herein, we use composites constructed via a pattern discovery technique involving "dynamic time warping" (DTW) and clustering, which we use to instead locate the most similar patterns of vortex evolution prior to SSWs. Using DTW allows us to detect patterns that are common across events, but that may occur at different lags relative to the SSWs themselves. In section 2 we introduce the datasets we use, and explain the DTW and clustering methods and our application of them to stratospheric polar vortex diagnostics. In section 3 we show the results of our analysis, and discuss them in the context of other work in section 4. Finally, in section 5 we summarize our main findings and results.

2. Data and methods

a. Reanalysis datasets and vortex diagnostics

We use the National Aeronautics and Space Administration's (NASA) Modern-Era Retrospective Analysis for Research and Applications, version 2 (MERRA-2; Gelaro et al. 2017), and the Japanese Meteorological Agency's (JMA) 55-year Reanalysis (JRA-55; Ebita et al. 2011; Kobayashi et al. 2015). We specifically use model-level products from these reanalyses as inputs to the Characterization and Analysis of Vortex Evolution using Algorithms for Region Tracking

(CAVE-ART) package described in Lawrence and Manney (2018). In brief, CAVE-ART uses computer vision techniques such as segmentation, region tracking, and edge tracing to characterize the stratospheric polar vortex. Using these techniques, CAVE-ART is able to track the genesis and lysis of vortex regions, and provide a set of vortex region and vortex edge diagnostics that are unique to these individual vortex regions (e.g., during vortex splits). We use the same MERRA-2 data described in Lawrence and Manney (2018), with additional years up through the 2017/18 Northern Hemisphere (NH) winter season added. For JRA-55, we have applied CAVE-ART to all NH winter seasons from 1958/59 to 2017/18, with vortex edges for JRA-55 calculated in the same manner as those for MERRA-2 (Lawrence and Manney 2018). Since JRA-55 does not provide a model-level PV product, we derive PV for it using the provided model-level wind components and temperature fields. More detailed information about these reanalyses can be found in Fujiwara et al. (2017). We primarily show results from JRA-55 herein because of its longer time record and more SSWs for study. We show one intercomparison later in the paper (see Fig. 2), and include all further MERRA-2 figures equivalent to the JRA-55 versions in the supplement.

b. Dynamic time warping and clustering

The goal of our analysis is to seek out patterns in vortex diagnostics prior to SSWs that could be indicative of preconditioning. However, we would like to not impose any constraints on how and when these patterns should appear; in other words, we want to seek out patterns without defining what they should look like beforehand, while also allowing for the possibility that any such patterns can occur at different lags and across different time scales relative to SSWs. For example, it is reasonable to expect that changes in the size of the vortex occur prior to SSWs, but we do not want to assume that, for example, the vortex only grows or shrinks, nor do we want to assume such patterns always occur sometime within 30 days of an SSW or at the same rate. For these reasons, we employ a clustering method in combination with dynamic time warping to perform pattern discovery.

DTW is a dynamic programming algorithm that "warps" the time dimension of a reference and input signal such that a given distance measure between the two is minimized. (Note, in discussing DTW, we often refer to "time series" and the "time" dimension for simplicity, but DTW is more generally applicable to other continuous or sequential data.) DTW accomplishes this by determining the sequence of index pairs (the "warping path" W^*) that minimizes the difference between the two input signals under a set of constraints (see the appendix). These index pairs theoretically map together similar features of the time series, such as peaks and troughs, that may occur with different amplitudes, at different time lags, and/or across different time scales. Thus, DTW is a pattern matching technique, since it better quantifies the similarity of signals regardless of such nonlinearities that may otherwise make them dissimilar if only compared at single instants in time (characteristics that have been referred to as "fuzziness"; e.g., Berndt and Clifford 1994). Figure 1 shows a schematic representation of these ideas. One may think of the way DTW works as similar to human understanding of speech despite subtle differences in the way words can be pronounced (indeed, DTW was developed for automated speech recognition; e.g., Itakura 1975; Reddy 1976; White and Neely 1976; Sakoe and Chiba 1978). The interested reader may see the appendix for more information about the formal foundations of DTW, and information about programming languages and packages that implement DTW; we also refer readers to Berndt and Clifford (1994) for more details about the technique and its applications for pattern discovery.

DTW matches patterns together in two individual sequences, but in applications with many sequences, other techniques such as clustering can be used in combination with DTW to detect specific patterns that arise within the database of sequences. In such cases,

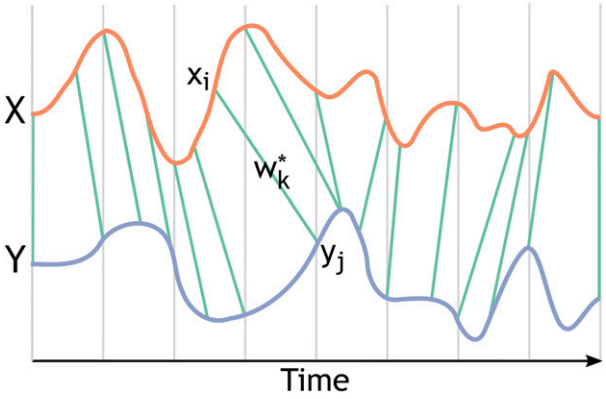

FIG. 1. A graphic representation of the DTW process, where X (orange) and Y (purple) are sequences defined over some interval (time in this example). The vertical light gray lines represent individual instants in time that correspond to the same time index of X and Y (e.g., x_i and y_i). The green lines represent the members w_k^* of the optimal warping path W^* that maps x_i to y_j such that the difference between X and Y is minimized (see section 2b and the appendix). Note that X and Y are artificially separated along the "y axis" for visualization purposes only, and that the w_k^* lines were hand drawn, and thus may not necessarily satisfy the DTW constraints that are typically imposed in practice.

the patterns detected are commonly referred to as ''motifs,'' as they are similar sequences repeated within a given dataset (e.g., Mueen et al. 2009). Most descriptions of DTW focus on 1D data, but DTW can also be applied to multidimensional datasets (e.g., Shokoohi-Yekta et al. 2017). Care must be taken when utilizing multivariate sequences in DTW to avoid issues with the ''curse of dimensionality'' (Verleysen and François 2005), which (in the context of DTW) refers to the tendency for data to become sparse in high-dimensional spaces, making distance measures become less useful (or virtually useless) for distinguishing similarity.

Herein, we perform multidimensional DTW on CAVE-ART time series from MERRA-2 and JRA-55, and perform simple nearest-neighbor clustering to locate motifs in vortex conditions prior to SSWs. We focus on three diagnostics from CAVE-ART that we use in the DTW and clustering: vortex area, vortex edge-averaged wind speeds, and vortex edge-averaged PV gradients. These diagnostics were chosen based on prior literature that discussed preconditioning in terms of changes to the vortex shape/size, sharpening of the PV gradients in the vortex edge region, and changes to the polar night jet (e.g., McIntyre 1982; McIntyre and Palmer 1983; Butchart and Remsberg 1986; Baldwin and Holton 1988; Albers and Birner 2014; Liu and Scott 2015). The DTW and motif-finding procedures are applied to each of these diagnostics separately (i.e., we do not consider the diagnostics all together as additional data dimensions); this was done to allow for the possibility that patterns in the different diagnostics could occur at different times relative to the other diagnostics and the SSWs themselves.

The CAVE-ART dataset consists of diagnostics that span from October 1 to May 1 of the next year, for all (October) years from 1959 to 2017 (1979–2017) for JRA-55 (MERRA-2). Given the relatively long radiative time scales in the lower and middle stratosphere (e.g., Newman and Rosenfield 1997), we attempt to find motifs with lengths of 30 days in the CAVE-ART data. Thus, we divide the raw CAVE-ART time series into sub–time series ''motif'' candidates, that each span 30 days (having lengths of 240 sampled at 8 times per day for MERRA-2, or 120 points at 4 times per day for JRA-55). Since we focus on conditions prior to SSWs, we only perform DTW on candidates that 1) are from years with major SSWs or ''major final warmings'' (as described next), and 2) have start dates between, at most, 90 and 30 days prior to the events (up to October 1 at the earliest). Regarding 1, we use dates listed in the SSW compendium table of events (see Butler et al. 2017) (located at https://www.esrl.noaa.gov/csd/groups/csd8/sswcompendium/majorevents.html; last visited September 2019). We also add a few additional dates to the pool of JRA-55 and MERRA-2 SSW dates: For years beyond 1980, we add SSW dates to MERRA-2 or JRA-55 if a given date is included in one reanalysis but not the other; this leads to the addition of 6 February 1981 and 4 March 1981 for MERRA-2 and 17 February 2002 for JRA-55. For years prior to 1980, we add 13 March 1969 to the JRA-55 pool, since this is considered a major SSW in both the NCEP–NCAR reanalysis and ERA-40. While such events are not classified as major midwinter SSWs across all the reanalyses, they still represent vortex disturbances that should be relevant for studying pre-disturbance vortex conditions. In addition to these, we also include the major SSW from 12 February 2018 (see Karpechko et al. 2018; Rao et al. 2018), and the anomalously early dynamically driven major final warmings from 12 March 2005 (Manney et al. 2006) and 6 March 2016 (Manney and Lawrence 2016). For years with multiple SSW events, the last event of the winter is chosen as the cutoff for the candidate sub–time series mentioned in 2 above.

All of the CAVE-ART vortex diagnostics are inherently multivariate as they are defined on multiple isentropic levels. Thus, to avoid issues with the curse of dimensionality, we perform DTW on the vortex diagnostics using only 3 CAVE-ART levels: 490, 800, and 1200 K, which characterize the lower- (~50–60 hPa), middle- (~10 hPa), and middle- to upper-stratospheric vortex (~3–5 hPa), respectively. The specific DTW procedure we use has been referred to as ''DTW_D'' (D for dependent), as all the dimensions are incorporated into the DTW procedure to determine similarity, as opposed to ''DTW_I'' (I for independent) that applies DTW to each individual dimension separately. Shokoohi-Yekta et al. (2017) provide more information on this distinction and argue that singular application of DTW_D or DTW_I can be problematic in some cases, but for our applications, we believe DTW_D makes the most sense physically. We z normalize the CAVE-ART diagnostics (i.e., subtract the sample mean and divide by the sample standard deviation, where the samples combine all available years together) on each isentropic level prior to performing DTW to ensure the calculations are invariant to scale and offset. Finally, since we must compute DTW distances for different combinations of dates in order to locate motifs, we reduce the space of possible combinations by only using candidates with 1200 UTC start times, and we disallow performing DTW between candidates that come from the same winter season.

To locate motifs, we adopt a simple nearest-neighbor clustering approach. Given the set of DTW distance

values for the many combined pairs of candidate sub–time series, we sort the values and require that any time series pairs' DTW value fall within the bottom 20% to be a candidate for a motif cluster. We begin with the minimum DTW value, which corresponds to the most similar time series pair—this is the first ''root'' pair, which forms the foundation for a cluster. We form clusters from root pairs by iteratively making sorted lists containing only DTW pairs that share a ''parent'' with any date already in the cluster (initially only the root pair), and adding the new date from the minimum DTW pair of this list. For example, if DTW(A, B) is the root pair, then we make a sorted (by DTW value) list of other DTW pairs having A or B as a member, and add the next minimum DTW pair of this subset [e.g., DTW(A, X) may be the next minimum, which would add X to the cluster and make the subsequent subset of potential members include pairs involving A, B, or X]. As dates are added to a cluster, we disallow the inclusion of further dates that are within 30 days of any already in the cluster. This process is repeated until no further candidates can be added. Additional clusters after the one formed from the first root pair are formed following the same procedure, but using new root pairs from walking through the sorted bottom 20% of DTW value pairs. Since we are attempting to locate and align vortex conditions that are similar across the greatest number of events, we select for consideration the cluster for each vortex diagnostic with the greatest number of members. In practice, the choice of our clusters are not very sensitive to ranking by reasonable weighted combinations of cluster-averaged DTW value and size of membership.

c. Statistical significance

In cases where we assess statistical significance of composite means of time series, we use a bootstrap resampling approach as follows: Given the number of members in our composites (each with equal length), and defining the members by their start dates (or day 0), we form N new composite means by taking a random selection (with replacement) of the start dates of our ''observed'' composite, and shuffling the years to any of those available within the reanalysis. We then catalog the $100 \times (\alpha/2)$ and $100 \times [1 - (\alpha/2)]$ percentiles of the N composite means and compare our observed composites to these values. Values exceeding these percentiles are considered to be significant at the α level. Herein we use $N = 100\,000$ and the $\alpha = 0.05$ level. Thus, for an example observed composite with 30 members, we would form 100 000 different 30-member time series composites with resampled dates and shuffled years, and points in our observed composite would be significant if they are less than the 2.5th percentile or greater than the 97.5th percentile.

3. Results

a. Motif and SSW-lagged composites

The motif composites (determined from the DTW and clustering procedure described in section 2b) for MERRA-2 and JRA-55 are compared in Fig. 2. Note that the time axes of the motif composites are not the same across all the diagnostics. In other words, day 0 for one diagnostic is generally not the same day 0 for another diagnostic, since the DTW and clustering processes were applied to each diagnostic and reanalysis separately. Despite the differences in sample sizes of clustered members between the two reanalyses, the composite averages shown in Fig. 2 and the intra-composite standard deviations (see Fig. 3 herein, and Fig. S7 in the online supplemental material) are very similar for both MERRA-2 and JRA-55. The general motif patterns shown by both reanalyses include a shrinking of the vortex, an intensification of wind speeds at the vortex edge, and an enhancement of PV gradients at the vortex edge. More specifically, the vortex area in the middle (lower) stratosphere shrinks (grows) such that the vortex goes from a roughly funnel shape (area increasing with height) to a roughly cylindrical shape (area constant with height). The vortex edge wind speeds accelerate most in the middle stratosphere above roughly 800 K, and reach peak intensity around day 20 of the motif period before decelerating thereafter. The two reanalyses differ most in the vortex edge-averaged PV gradients, particularly in the magnitude of values [which have units of $10^{-7}\,s^{-1}\,km^{-1}$ from scaling the PV as in Dunkerton and Delisi (1986)]. Qualitatively, the vortex edge PV gradients evolve similarly in both datasets, with gradual increases over the 30-day motif periods. Structurally, however, MERRA-2 tends to have the largest vortex edge-averaged PV gradients in the 800–1100 K layer, whereas JRA-55 tends to have the largest gradients above 1100 K. These differences in the reanalysis vortex edge PV gradients are discussed in more detail in the conclusions. Examination of the specific dates included in the clusters show that in the shared period of 1979/80–2017/18, the dates chosen in the clusters tend to be only 1–3 days different between the reanalyses, but on occasion can be different by as much as 7–10 days. There can also be some dates included/missing in one reanalysis, but not the other. However, the motif patterns for both JRA-55 and MERRA-2 remain robust regardless of whether only years post-1979 are included, and/or whether the motif dates are swapped between the reanalyses (not shown).

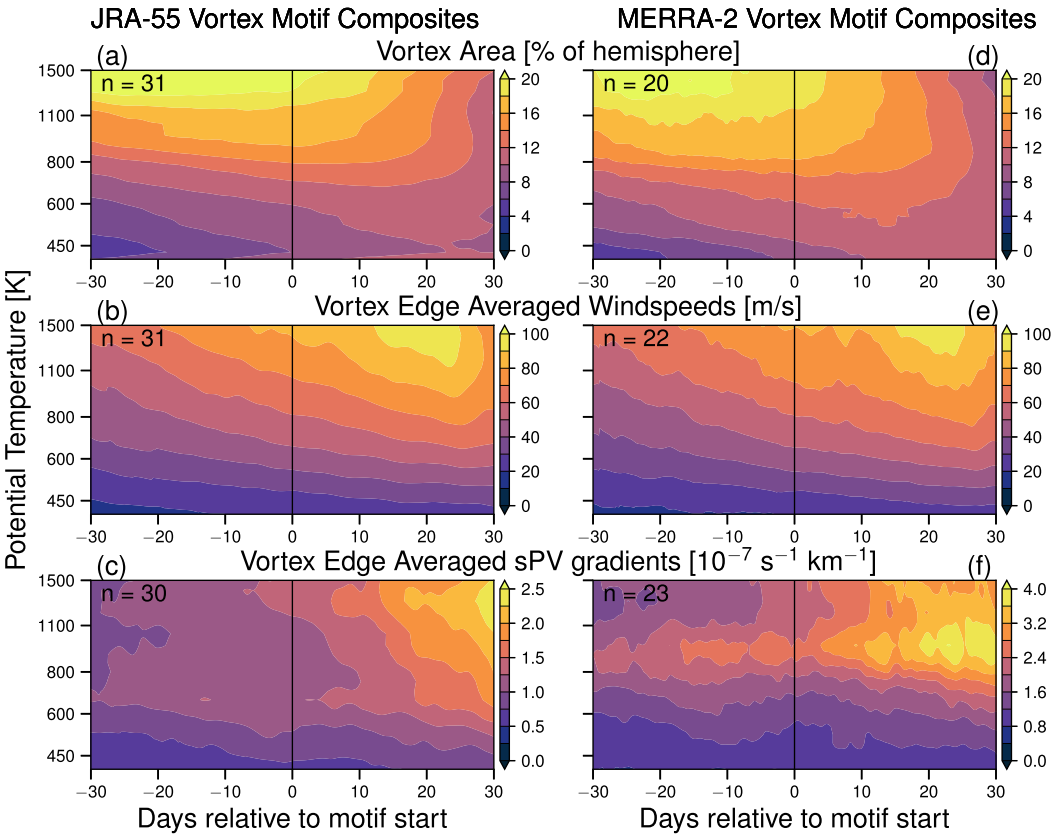

FIG. 2. Composite means of vortex motifs calculated using (a)–(c) JRA-55 and (d)–(f) MERRA-2 data, for days −30 to 30 relative to the motif start dates (vertical black lines).

Please see the Figs. S1–S6 for graphs of the specific dates found through the clustering procedure.

Figure 3 shows the motif composite from JRA-55 with composite means and standard deviations side by side with lagged composites relative to the central date of SSWs (including the major final warmings discussed in section 2b). The composite means between the motif and SSW-lagged composites show similar features: In the SSW-lagged composites, the area diagnostic shows a shrinking of the vortex; vortex edge-averaged wind speeds show acceleration prior to a period of deceleration; and vortex edge-averaged PV gradients increase leading up to the central date of the SSWs. However, there are notable differences in when such signals are apparent in the SSW-lagged composites. For example, the maximum vortex edge-averaged wind speeds in the SSW-lagged composite occurs between the −25- and −20-day marks, whereas it occurs in around the +20- to +25-day marks in the motif periods, suggesting that the motif period may often fall in the −45- to −15-day time frame prior to SSW events. The largest differences lie in the intracomposite standard deviations. The motif composite standard deviations are notably reduced in comparison to those for the SSW-lagged composite, in both the 30 days prior and the 30 days during the motif periods. The only exception is in the vortex edge-averaged PV gradients above 800 K, in which the motif composite standard deviations are of a similar magnitude to those in the SSW-lagged composite. These results suggest that the variability among the clustered events is reduced by the DTW and clustering procedure better "aligning" these vortex features in time (i.e., matching the patterns together).

Figure 4 compares the motif and SSW-lagged composites in terms of averaged standardized anomalies. As expected based on Fig. 3, the structures in the anomalies are similar between the two composites in all the diagnostics. In the motif composite, the vortex area panel shows that the vortex grows to be anomalously large from roughly 800 K and above between −30 and +10 days, before it shrinks to anomalously small values. The vortex also grows to anomalously large values below 800 K in the lower stratosphere, indicating that the evolution toward a more "cylindrical" shape shown in the motif vortex area composite of Fig. 3 is a combination of growing and shrinking at different

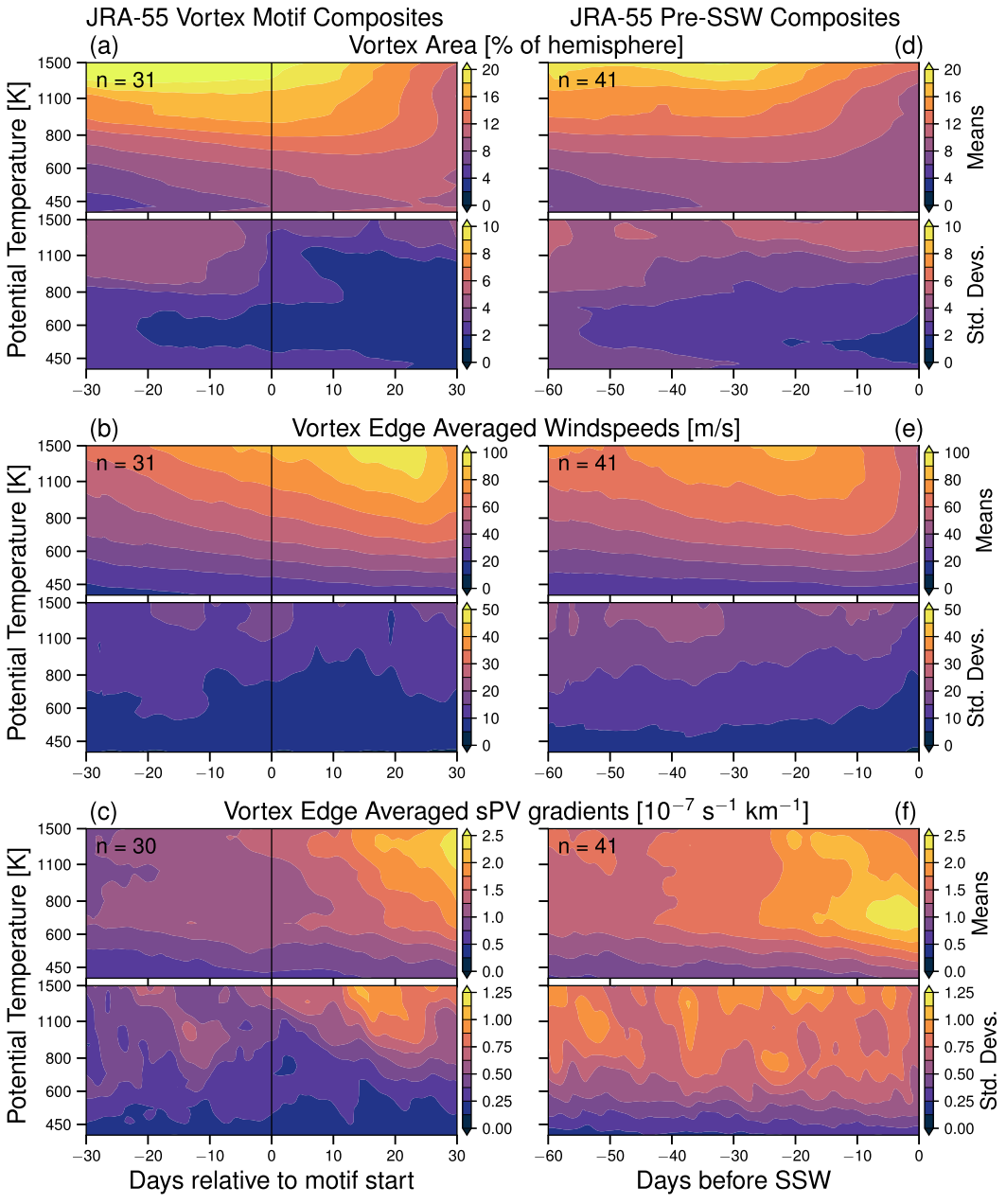

FIG. 3. (a)–(c) Composite means and standard deviations of vortex motifs relative to motif start dates compared to (d)–(f) lagged composite means and standard deviations relative to the central dates of SSWs from JRA-55.

altitudes. The vortex area anomalies evolve similarly in the SSW-lagged composite, but the time scale is much more confined to roughly 35–30 days prior to the SSWs, whereas the motif composite reveals the process occurs over nearly 60 days. Both of the vortex edge-averaged wind speed composites show that winds tend to be anomalously strong prior to SSWs, but in the motif composite, the winds are shown to be much stronger through a greater depth of the stratosphere. The greatest differences between the motif and SSW-lagged composites are seen in the vortex edge-averaged PV gradients. While both composites show an increase to anomalously high PV gradients beginning at levels in the middle to upper stratosphere, the motif composite also shows that the PV gradients at the vortex edge are often initially anomalously weak in the lower and middle stratosphere.

The results from Figs. 2–4 agree well with previous studies that discussed preconditioning prior to SSWs.

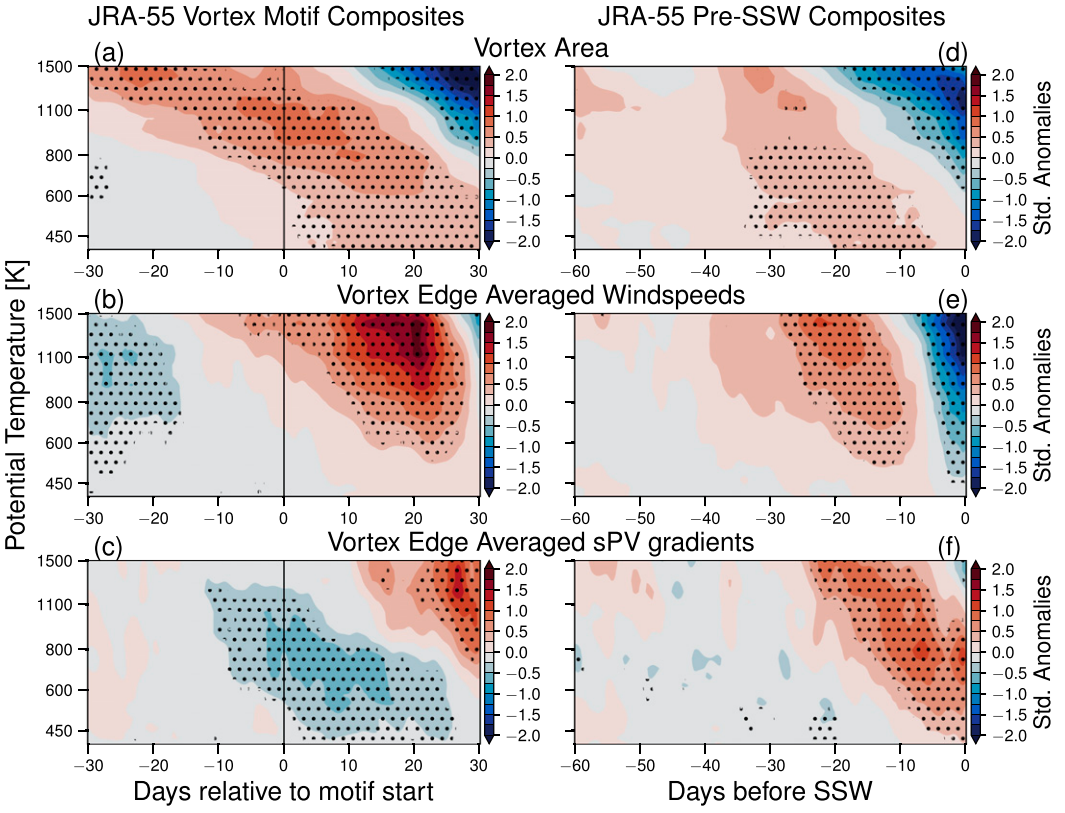

FIG. 4. (a)–(c) Motif vs (d)–(f) SSW composites from JRA-55 as standardized anomalies of vortex diagnostics. Stippling indicates statistical significance at the 0.05 level determined from a bootstrap resampling procedure.

While only about 75% of the total number of SSW events are represented in the clustered motifs, the composites show a clearer picture of vortex evolution compared to the SSW-lagged versions. The decrease in vortex area seen in the middle to upper stratosphere of both the motif and lagged-SSW composites is consistent with the predictions of McIntyre and Palmer (1983) and the findings from Baldwin and Holton (1988) that the vortex shrinks prior to SSWs. These results also show that PV gradients tend to sharpen in the vortex edge region prior to SSWs, which agrees with prior studies that discuss this as a characteristic of preconditioning (McIntyre 1982; McIntyre and Palmer 1984; Albers and Birner 2014; Liu and Scott 2015). Interestingly, Fig. 4 shows that vortex edge PV gradients are often anomalously weak before the sharpening at all levels, which could be important in light of the results from Scott et al. (2004) discussing how weak (strong) PV gradients in the lower stratosphere can inhibit (support) vertical wave propagation. Limpasuvan et al. (2004) found anomalously strong zonal winds poleward of 70°N in the onset phase of SSWs; given a reduced vortex size, the strong vortex edge wind speeds shown in Fig. 2 could be consistent with this result if the vortex was relatively pole centered such that the edge winds were mostly zonal. These anomalously strong edge wind speeds also agree with the finding in Lawrence and Manney (2018) that vortex edge wind speeds are often anomalously strong prior to SSWs.

Figure 5 shows the difference between the end dates of the 30-day motifs and the central dates of the considered SSWs for each of the diagnostics. These quantities give an idea of the approximate lead time the motif patterns are fully apparent in each of the diagnostics before the definition of a sudden warming is met. Figure 5 also shows the events for which no motif(s) were found; generally these are from winters with two SSWs, with one SSW being ''captured'' and the other not. Note that this does not necessarily mean there were no signs of preconditioning in these cases, just that the patterns preceding such events were not similar enough to be clustered based on our requirement for similarity. There is apparent large variability in lead times from event to event, but usually the vortex edge-averaged PV gradient motifs precede the edge-averaged wind speeds and vortex area motifs, often by more than 10 days. The median lead times for JRA-55 motifs are 22.5, 10, and 9 days for vortex edge-averaged PV gradients,

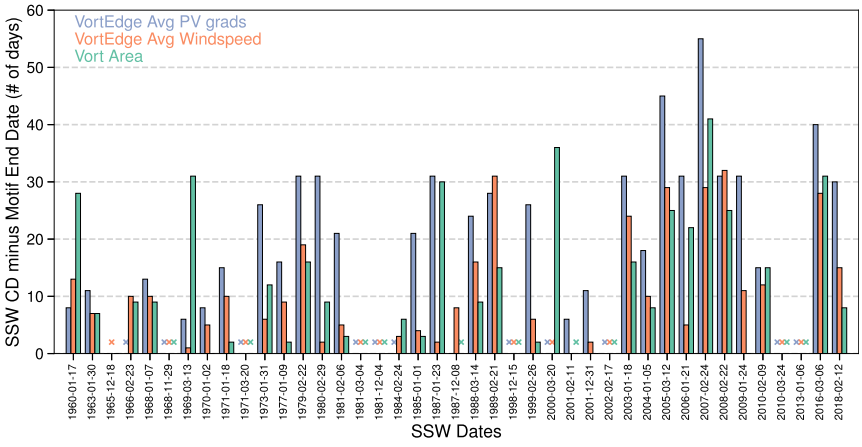

FIG. 5. Bar plot of motif end dates from JRA-55 relative to SSW central dates for the three vortex diagnostics: vortex edge-averaged PV gradients (purple), vortex edge-averaged wind speeds (orange), and vortex area (green). Crosses indicate cases where no motif was found or could be connected to the given event. Cases where there are no crosses or bars have lead times near or less than 0 (from cases with multiple SSWs in a winter). The most negative lead time is −7 days for JRA-55 on 8 Dec 1987.

edge-averaged wind speeds, and area, respectively (24, 9, and 7.5 days, respectively, for the same quantities based on MERRA-2). There are also many cases in which the lead time of the motifs, particularly those for the vortex edge-averaged PV gradients and vortex area, are apparent by more than 20–50+ days relative to major warmings. Given that the distribution of potential vorticity is directly influenced by diabatic heating effects (Butchart and Remsberg 1986; Nash et al. 1996; Kwasniok et al. 2019), and that radiative time scales throughout the stratosphere are generally less than 20–30 days (Newman and Rosenfield 1997), it is possible that the patterns evident in the motifs, particularly those associated with the vortex area shrinking and edge PV gradients sharpening, may not stay consistent in such long-lead cases.

To examine this further, Fig. 6 shows composites of the subsets of these long-lead cases, binned by motifs having lead times within 20–29, 30–39, 40–49, or 50–59 days. The vertical black lines plotted on each panel show day 30 (the end date) of the motifs, and the later date by which an SSW must have occurred for the particular bin. Despite the small sample sizes, the composites do demonstrate a degree of persistence among the motif patterns. The vortex edge-averaged PV gradients show the pattern of sharpening and downward tilting contours in the first 30 days, but then stay enhanced throughout the majority of the potential temperature range. In the 50–59-day lead bin of the vortex edge-averaged PV gradients, there is a single composite member that shows two sharpening events in the middle to upper stratosphere; this member comes from the 2006/07 winter with a major SSW on 24 February 2007. The motif pattern detected in this case captures the first sharpening event when the lower stratospheric PV gradients are weak, as opposed to the later ''resharpening'' that occurs primarily in the upper levels while the lower stratospheric gradients remain enhanced. This event also comprises the single composite member in the vortex area 40–49-day lead bin, which shows the signs of a brief vortex recovery in the upper levels as evidenced by the growth in area around day 40 relative to the motif start date. This vortex recovery and double-edge sharpening event occurred in the aftermath of two minor warmings that primarily affected the upper stratosphere, where zonal-mean zonal winds dipped to approximately $15\,\mathrm{m\,s^{-1}}$ at pressures lower than 5 hPa (not shown). The other composites of the long-lead vortex area motifs show a similar persistence in that the shrinking of the vortex either continues or remains held until the SSWs occur. All three of the vortex area composites show that the size of the vortex is quite uniform with altitude (excepting the signs of growth in the upper levels associated with other temporary ''recoveries''), on the order of 10%–12% of a hemisphere throughout the altitude range. The vortex edge-averaged wind speeds only have cases in the 20–29- and 30–39-day lead bins, and even in the latter, the two members of the composite have lead times closer to 30 days (see Fig. 5). These composites show that following the acceleration of the polar night jet that primarily comprises the motif pattern, the wind speeds become relatively constant in the middle and lower stratosphere until the time of the major warming.

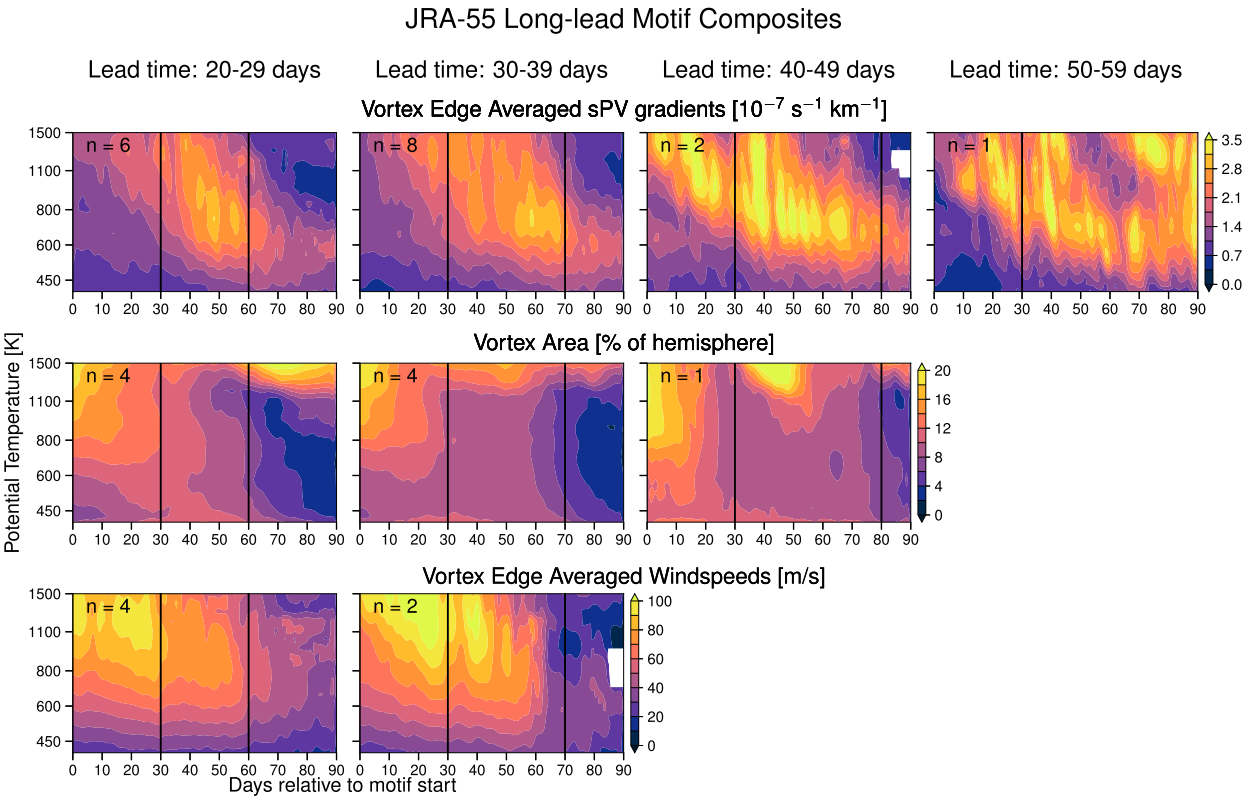

FIG. 6. Subcomposite means of vortex diagnostic motifs in cases with long leads, binned by (left to right) 20–29, 30–39, 40–49, and 50–59 days. The first vertical black lines indicates the 30-day ''end points'' of the motifs found through the DTW and clustering procedure, while the second black vertical lines indicates the time by which an SSW must have occurred for the given lead-time bin.

Figures 5 and 6 demonstrate that the vortex characteristics described by the motifs not only occur at different times relative to SSWs, but that they can also be maintained across different time scales. This suggests that there exists a spectrum of pre-SSW time scales from ''more sudden'' SSWs in which the motif patterns arise as part of the development of the SSW (i.e., in which the motif end dates are close to the SSW central dates), to more prolonged events in which the motif patterns arise early and remain somewhat frozen-in. The fact that the vortex edge PV gradient motifs often are apparent earlier in time relative to SSWs than the motifs for vortex area and edge wind speeds (as shown in Fig. 5) also seems to agree with theoretical considerations: Sharpening of PV gradients, particularly at lower levels, should act to enhance wave driving and wave breaking (Scott et al. 2004). These processes in turn influence the size and strength of the vortex, so sharpening of PV gradients should tend to precede such other signals (Jucker 2016).

It is natural to ask whether there are any differences in the pre-SSW motifs related to whether the later disturbances are splits versus displacements. Charlton and Polvani (2007) identified key differences in the stratospheric and tropospheric circulation prior to split and displacement SSWs. Similarly, Bancalá et al. (2012) found unique signatures prior to wave-1 versus wave-2 SSWs that were related to Euro-Atlantic versus Pacific blocking in the troposphere. Albers and Birner (2014) even suggested there should be separate definitions of preconditioning for displacement versus split SSWs that reflect the geometries necessary to trigger SSWs of the two types. We provide figures in the supplement (see Figs. S11 and S12) that show our pre-SSW motif composites subdivided by whether the eventual disturbances were splits or displacements. We do not see evidence to suggest there are important differences in the patterns or lead times of the three diagnostics we consider here when composited by the type of eventual SSW. Furthermore, when expressed as anomalies (not shown), the subsetted split and displacement motif composites look very similar to the results shown in Fig. 4, indicating similar vortex evolution with respect to the climatology. However, these results do not rule out the possibility of there being relevant signals in other dynamical or geometrical vortex diagnostics (such as those shown in, e.g., de la Cámara et al. 2019). There could also be a sampling effect related to there being more cases with no motifs

associated with displacement SSWs (i.e., a larger fraction of the total number of split events are represented in the motifs than the displacements).

b. *Years without major SSWs*

It would be remiss not to examine years that did not have major SSWs. For one thing, we have included events in our analysis that are not considered SSWs by standard definitions (e.g., the dynamically driven final warmings mentioned in section 2b), as well as cases that qualify as major SSWs only in some reanalyses, but not others. It is well known that different definitions for SSWs can affect the frequency of detected events ranging from roughly 4 to 10 events per decade (i.e., nearly an event every year; Butler et al. 2015; Palmeiro et al. 2015). There is also significant intra-SSW variability in terms of how much the polar vortex actually becomes disturbed or broken down throughout the stratosphere (Lawrence and Manney 2018). Some have argued that stratospheric warmings form a continuum (Coughlin and Gray 2009; Maury et al. 2016) of which "major" SSWs are only a part of a tail of the distribution. Indeed, there have been events such as those that occurred in February 2017 in which there were two separate strong decelerations of the stratospheric circulation such that zonal-mean zonal winds got within 1–2 $m\,s^{-1}$ of a complete reversal at 10 hPa and 60°N latitude. Furthermore, the processes that are slated to precondition the vortex are essentially minor warming events, which are common in the NH polar winter stratosphere. For these reasons, we extend our use of DTW to winters without major SSWs defined by the Charlton and Polvani (2007) definition, on which the SSW compendium is based (Butler et al. 2017).

Since we already have a set of motifs defined with clustering using pre-SSW vortex conditions, we simply use our detected motifs as "templates" to use DTW to search through years without major SSWs for time series that optimally match with our detected motifs. This amounts to selecting dates that correspond to local minima in the DTW similarity measures that fall within the bottom 20% of similarity (defined from years with SSWs) with at least one of the pre-SSW motifs, with the requirement that multiple local minima from a single winter be separated by at least 30 days. For simplicity, we will refer to these cases as "non-SSW motifs."

Figure 7 shows the non-SSW motif composites as both raw diagnostic values and standardized anomalies (cf. the left and right columns of Fig. 7 to the left columns of Fig. 2 and Fig. 4, respectively). The raw non-SSW motif patterns are very similar to the pre-SSW motif patterns seen in Fig. 2, with a shrinking vortex area (Fig. 7a), a strengthening jet (Fig. 7b), and sharpening edge PV gradients (Fig. 7c). In some ways this is not too surprising since we specifically used the pre-SSW motifs to locate similar patterns in years without SSWs. However, the sample sizes of the composites for each of the diagnostics are also similar—roughly 30 for JRA-55 and roughly 18 for MERRA-2. In combination with the pre-SSW motifs, motif patterns are found in over 90% of Northern Hemisphere winters (92%–95% based on JRA-55 diagnostics). The non-SSW motif patterns as anomalies are also similar to the pre-SSW patterns, but generally less pronounced. The one exception is in the non-SSW vortex edge-averaged wind speeds, which are anomalously strong across the levels for nearly the whole 30-day motif period.

To examine whether these non-SSW motif patterns are associated with later vortex disturbances that do not meet the Charlton and Polvani (2007) definition, we seek other "significant disturbances" (SDs) by searching for cases where daily averaged zonal-mean zonal winds at 10 hPa and 60°N dip below 10 $m\,s^{-1}$ between 1 December and 15 March, and defining central dates of SDs as the dates of the minimum zonal wind values below this threshold. We choose 10 $m\,s^{-1}$ as a simple and convenient threshold as it is weak relative to climatology throughout the 1 December–15 March period (between roughly the 10th and 30th percentiles). For potential central dates in March, we additionally require that they be separated from the final warming (the date when zonal-mean zonal winds at 10 hPa and 60°N reverse to easterly and do not recover thereafter) by at least 20 days. This additional constraint is to control for the 10 $m\,s^{-1}$ threshold becoming less of an anomaly in late winter, and because there are several early final warmings, particularly in the pre-1979 JRA-55 record (e.g., Hu et al. 2014), for which we do not attempt to evaluate whether they were dynamically driven (we note, however, that roughly 40% of the years with non-SSW motifs are winters with March final warmings). We emphasize that we are simply using the zonal winds to find other anomalous vortex disturbances, not attempting to introduce another definition of SSWs. Table 1 shows the list of the dates found; for years beyond 1979, MERRA-2 and JRA-55 both give equivalent dates. There are 16 SDs in the JRA-55 record, 12 of which are also in the MERRA-2 record. This indicates that at most, approximately 53% of the non-SSW motifs from JRA-55 (67% for MERRA-2) can be associated with the SDs.

By linking these SDs to the nearest non-SSW motifs from the same season, we can similarly examine the approximate lead times of the non-SSW motifs. This is shown in Fig. 8 as histograms of the pre-SSW motif lead times, with non-SSW (SD) lead times stacked on for

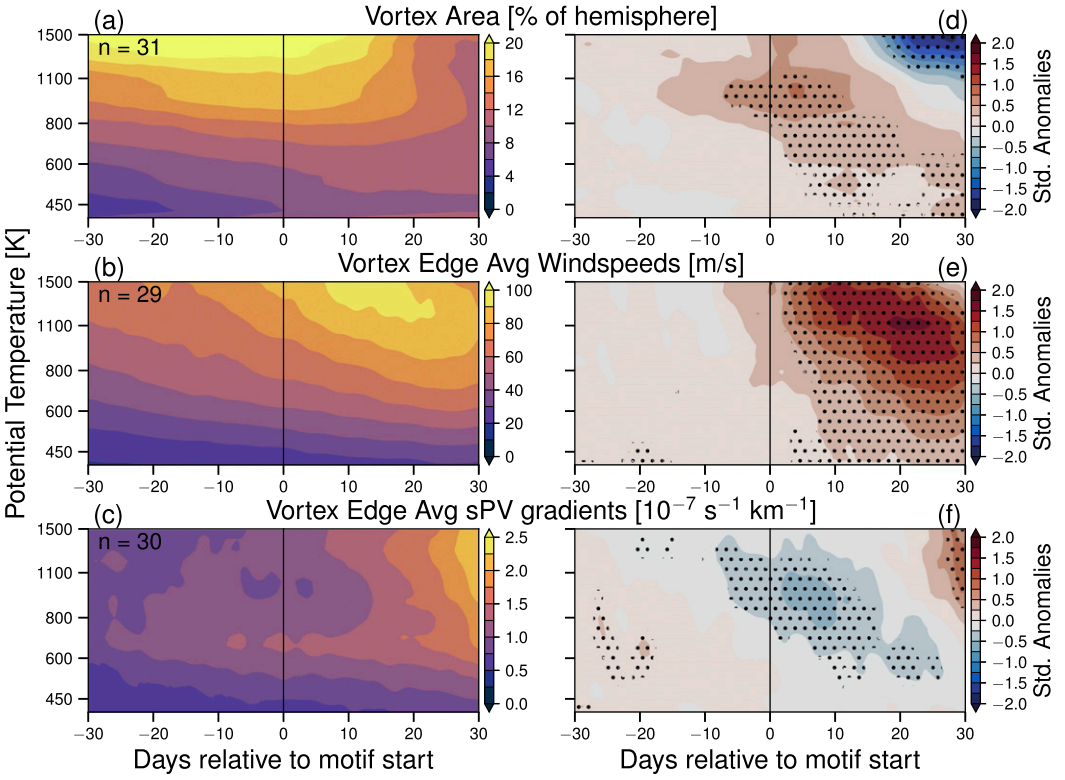

FIG. 7. Non-SSW motifs from JRA-55 as composite means of (a)–(c) the raw diagnostic values and (d)–(f) the standardized anomalies.

each of the vortex diagnostics. In general, including the non-SSW motif lead times with those from the pre-SSW motifs has little effect on the shapes of the distributions, and this is reflected in the medians of the distributions staying relatively invariant: For JRA-55 (MERRA-2), including the lead times of the non-SSW motifs changes the medians from 22.5 to 26 (24 to 24.5) days for vortex edge-averaged PV gradients, from 10 to 10 (9 to 9) days for edge-averaged wind speeds, and from 9 to 9 (7.5 to 9) days for vortex area. For the pre-SSW motifs, it was only possible to get "negative" lead times (relative to the motif end dates) in cases where there were two SSWs in a particular winter season. With the non-SSW motifs, we performed no cutoffs of allowable time series, and thus there are a couple of additional negative lead time cases. There are also a few additional long-lead non-SSW motifs (leads greater than 20 days), particularly for the vortex edge-averaged PV gradients. An investigation of the persistence of patterns such as PV gradient sharpening and shrinking vortex area similar to that shown in Fig. 6 indicates that such patterns are also maintained over these periods.

Since signs of preconditioning are themselves thought to arise as a result of minor warming–like disturbances, we examine whether there are discernible minor warming signals associated with the non-SSW motifs. Figure 9 shows pressure–time series composites of the time derivatives of 60°–90°N polar cap–averaged temperatures and zonal-mean zonal winds at 60°N averaged in the

TABLE 1. Table of "significant disturbance" central dates, defined in section 3b. Minimum zonal wind values for years after 1979 are the average of the values obtained from MERRA-2 and JRA-55.

Central dates	Associated minimum U at 10 hPa and 60°N (m s^{-1})
3 Dec 1958	1.16
18 Dec 1960	7.11
27 Feb 1972	4.92
31 Jan 1978	9.23
27 Feb 1983	4.56
12 Feb 1990	7.97
29 Jan 1991	7.22
19 Jan 1992	9.25
9 Mar 1993	1.03
2 Jan 1994	3.40
5 Feb 1995	0.43
14 Mar 1996	9.59
8 Jan 1998	1.58
23 Jan 2012	6.87
1 Feb 2017	1.49
26 Feb 2017	1.00

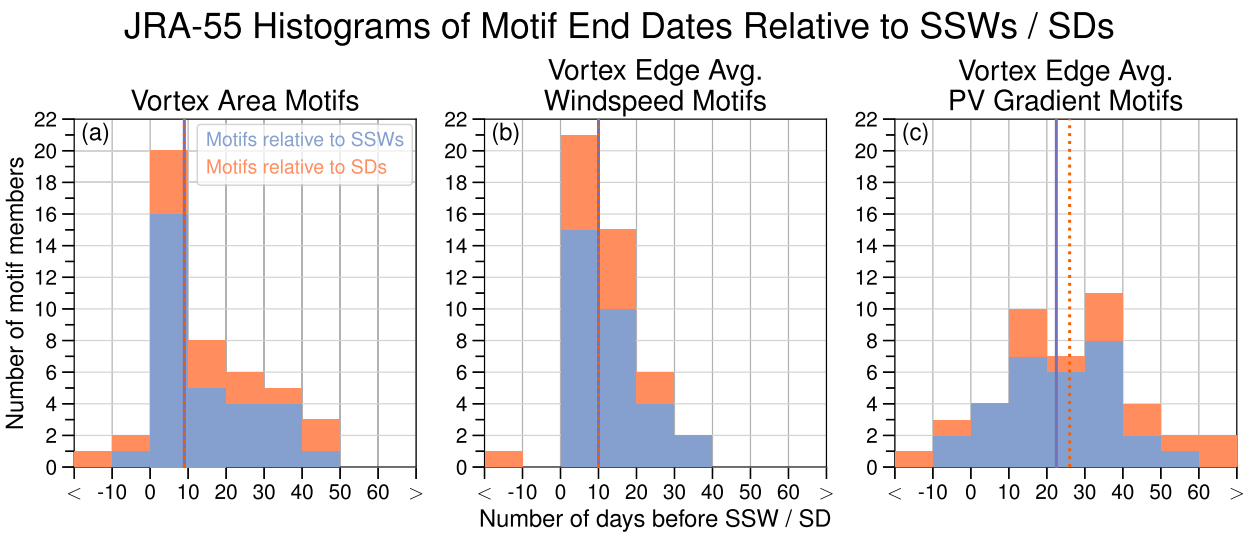

FIG. 8. Stacked histograms of motif lead times relative to sudden stratospheric warmings (SSWs) and "significant disturbances" (SDs). The purple bars represent the lead times for motifs relative to SSWs only, while the orange bars represent the lead times of non-SSW motifs relative to the SDs. The darker purple and orange vertical lines indicate the medians of the distributions when only considering SSWs and when considering both SSWs and SDs, respectively. The orange lines are dashed to be able to see the purple line when both medians are equal.

non-SSW motif periods. For the vortex area and edge-averaged wind speed composites, there are notable warming and deceleration signals within the 30-day motif periods. For vortex area, the strongest warming and deceleration tends to occur around days 10–15 of the motifs, around the time when the vortex area begins to decrease most rapidly in the middle to upper stratosphere (Figs. 7a,b). In the edge-averaged wind speed motif composites, the strongest warming and deceleration instead occurs between days 25 and 35, coincident with the time when vortex edge wind speeds begin to decelerate throughout the stratosphere (Fig. 7c); however, there is also a recovery signal thereafter with significant cooling and acceleration of the zonal winds, particularly in the middle to upper stratosphere. The edge-averaged PV gradient composites show weaker and less statistically significant signals, but there is a general coherent warming trend centered between days 20 and 30, at the time when PV gradients in the middle to upper stratosphere rapidly sharpen (Figs. 7e,f). There is also a second coherent warming signal around day 37 associated with a brief statistically significant deceleration. These results demonstrate there is a strong association between the motif signals that show signs thought to be indicative of preconditioning and minor warmings confined to the middle and upper stratosphere. While such results do not prove a direct causative relationship, minor warmings are primarily associated with the appearance or transient strengthening of anticyclones in the stratosphere such as the Aleutian high (e.g., Colucci and Ehrmann 2018), which are often responsible for wave breaking on the edge of the vortex. Minor warmings could therefore be important as controlling mechanisms that modify the risk of later larger vortex disturbances such as SSWs, and perhaps also dynamically driven final warmings.

4. Discussion

Decreased vortex area and sharpened edge PV gradients have sometimes been discussed as signs of a preconditioned vortex because of "wave focusing" arguments; a smaller vortex with sharp PV gradients in the edge region helps to guide vertically propagating planetary waves along and into a smaller and less massive vortex region that can be more strongly influenced (McIntyre 1982; McIntyre and Palmer 1983). Enhanced PV gradients in the vortex edge region in the lower stratosphere have additionally been shown to have a controlling effect on the vertical propagation of waves into upper levels (Scott et al. 2004). A reduction in vortex area and enhanced PV gradients in the vortex edge region have also been discussed as signs of preconditioning in the context of resonant triggering of SSWs as parameters that can influence bringing the vortex closer to resonance, albeit primarily in the context of vortex split SSWs (Albers and Birner 2014; Liu and Scott 2015; Scott 2016). For simplicity we refer to these two characteristics (decreased vortex area and

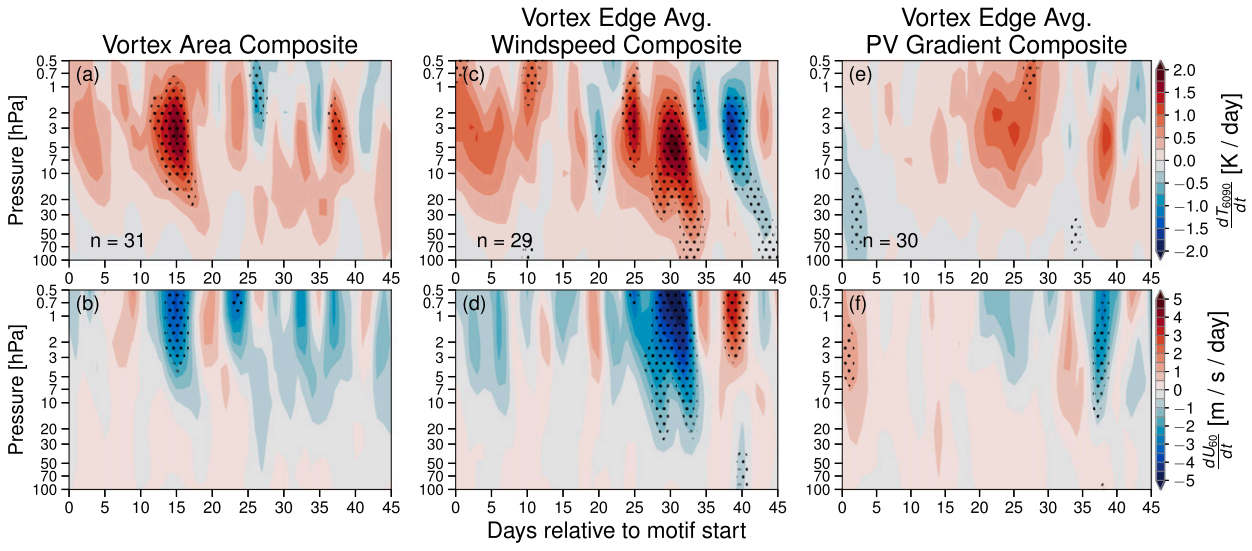

FIG. 9. Composites of the time derivatives of polar cap (60°–90°N)–averaged (a),(c),(e) temperatures and (b),(d),(f) zonal-mean zonal winds at 60°N from JRA-55 averaged in the non-SSW motif periods from 0 to 45 days relative to the motif start dates.

enhanced edge PV gradients) as the ''canonical signs'' of preconditioning. Changes to the strength of the polar night jet have been discussed as being indicative of ''jet sharpening'' and relevant to preconditioning via gravity wave drag (GWD) (Albers and Birner 2014), since gravity wave amplitudes and momentum fluxes have been found to be strongest near the core of the jet where winds are strongest (Wang and Alexander 2009; Ern et al. 2016; Plougonven et al. 2017). As discussed previously, the pre-SSW motifs found herein do show the canonical signs of a shrinking vortex (particularly in the middle and upper stratosphere) and sharpening PV gradients in the vortex edge region. Additionally, the vortex edge wind speed motifs show a strong acceleration leading up to a relatively short and abrupt deceleration that levels off the wind speeds. In terms of anomalies, the reduction in area leads to an anomalously small vortex in the middle and upper stratosphere, simultaneous with a larger than normal vortex in the lower stratosphere. PV gradients in the lower stratosphere are anomalously weak until late in the motif period when gradients become anomalously strong in the middle and upper stratosphere. The vortex edge-averaged PV gradient motifs also usually have the longest lead times preceding vortex disturbances; the median lead times relative to disturbances were about 25 days [consistent with the time scale on which Jucker (2016) found PV gradients sharpened], while those for the vortex area and edge wind speeds were about 10 days. This suggests an approximate 2-week lag between the vortex edge PV gradient and wind speed/area motifs (i.e., day 0 of the wind speed/area motifs would be about day 15 of the PV gradient motifs).

The above suggests a schematic interpretation: Early on (relative to a later disturbance) when PV gradients in the vortex edge region are weak in the lower stratosphere, vertical wave propagation along the vortex is mostly inhibited. As these gradients increase, increasingly more wave propagation is guided aloft where wave breaking can occur in the upper stratosphere regardless of the edge PV gradients there (Scott et al. 2004). As more wave breaking aloft occurs, the size of the vortex is reduced, upper-level PV gradients in the edge region become enhanced, and jet sharpening increases the relative strength of the jet. By this point, the vortex could be said to be preconditioned in that the canonical characteristics are present. However, the triggering of an SSW or significant disturbance does not have to happen immediately thereafter, since we showed that these canonical characteristics can be maintained for long periods of time. This suggests that whatever comes next, whether it be anomalously large wave forcing supplied by the troposphere, nonlinear feedbacks, or resonance effects, the processes evolve according to the prior redistributions of the PV field, which implies it should act as a sort of memory [similar to the ''noise-memory paradigm'' discussed by Esler and Mester (2019)]. Our results further suggest that some SSWs and vortex disturbances may be more sudden than others in that with some events, the canonical signs may arise as a continuous part of the evolution toward the SSW itself (i.e., in cases with motif lead times close to 0 days).

The fact that we found similar vortex characteristic motifs in virtually every year without major SSWs may seem concerning. Preconditioning has often been discussed only in the context of major SSWs. Smith (1992) discussed some possible distinctions in interpretations of preconditioning: either preconditioning requires an additional ingredient that when added leads to a major warming, or an identified preconditioned state is evidence of a major warming already underway. The former interpretation implies preconditioning is a necessary but insufficient condition for a major warming, while the latter makes preconditioning inseparable from the major warmings themselves. Our results support the former interpretation, that preconditioning alone does not guarantee the occurrence of an SSW. Precursor wave pulses and wave breaking on the vortex edge have typically been discussed in the literature as leading to the canonical signs of preconditioning, and such events are common in the Arctic wintertime stratosphere. Indeed, we showed that there appears to be a strong association between the motifs in years without SSWs and basic signals of minor warmings such as polar cap warming and zonal wind decelerations (Fig. 9). Further, we also showed that in many of these winters, there go on to be later significant disturbances that do not quite meet common major SSW definitions. A definition of preconditioning inextricably tied to major warmings would require a possibly presently unknown definition of major warming that would be able to unambiguously distinguish between, for example, cases where 10-hPa, 60°N zonal-mean zonal winds reverse to easterly for over 10 days (such as the recent February 2018 event), approximately a single day (such as the event from January 2003), and events that get within roughly $1\,\mathrm{m\,s^{-1}}$ of a total reversal (such as the event from February 1995), as well as details of when and why preconditioning only exists for the ''true'' major warming(s).

While an in-depth analysis of the potential ''extra ingredient'' to preconditioning is beyond the scope of this study, we can discuss some possibilities. Our results in section 3b made the distinction between major SSWs and significant disturbances, so we can also examine years without either. Figure 10 shows composites of anomalies in the upward component of the Eliassen–Palm flux (Andrews et al. 1987) provided in the zonal-mean dataset of reanalyses by Martineau et al. (2018b), with years for 2017 and 2018 filled in separately using the same methods (since the zonal-mean dataset presently only provides data up through 2016 for JRA-55 and MERRA-2). The composites are plotted in the vortex area motif periods for years with major SSWs, years with SDs, and years with neither. In the SSW composite (Fig. 10a), there is a prolonged period of time between roughly days 10 and 40 when upward wave activity is enhanced in the stratosphere. For the composite of SDs (Fig. 10b), there are two separate periods of enhanced (but less pronounced) upward wave activity in the stratosphere centered on 10 and 30 days. In contrast, in the composite without SSWs or SDs, there are prolonged periods with anomalously low wave activity in the stratosphere between 20 and 60 days (relative to the vortex area motifs). While it is well known that vortex disturbances can occur without anomalously high wave fluxes supplied by the troposphere (e.g., Jucker 2016; Birner and Albers 2017; de la Cámara et al. 2019), the composite without SSWs or SDs seems to indicate that wave activity in the stratosphere in these cases was anomalously low. This could suggest that after some form of preconditioning took place, the supply of wave activity from the troposphere was less than normal in these cases. Alternatively (or in combination), there could be some processes in the lower/lowermost stratosphere that controlled and inhibited wave propagation into the stratosphere. Indeed, the concept of preconditioning of the vortex could possibly benefit from more clearly elucidating the role of lower levels in the stratosphere; preconditioning has primarily been discussed as processes affecting the middle stratospheric vortex, when in contrast, many studies have consistently noted a connection to, or control of, SSWs by the lower stratosphere (e.g., Smith 1992; Chen and Robinson 1992; Scott and Polvani 2006; Birner and Albers 2017; Martineau et al. 2018a).

Smith (1992) also posed another interesting and related question about whether preconditioning could be usefully defined by a threshold that must be surpassed for a major warming to be triggered, or whether there are degrees of preconditioning that depend on multiple parameters. These ideas do not seem mutually exclusive since the former idea would require a definition of ''preconditioned enough.'' Our findings provide support for the idea that preconditioning is a continuous rather than a binary process simply because we found motifs exhibiting the canonical signs of preconditioning prior to SSWs, prior to significant disturbances, and in cases without either. There seems to be support for this notion elsewhere—for example, de la Cámara et al. (2017) clearly demonstrated that the occurrence of major SSWs depended on prior stratospheric conditions. However, many of the ensemble members of the various experiments they performed that did not evolve toward major SSWs still went on to evolve toward what could be considered significant disturbances; see for example, the non-SSW (blue) vortex edges in their Fig. 7 that go on to

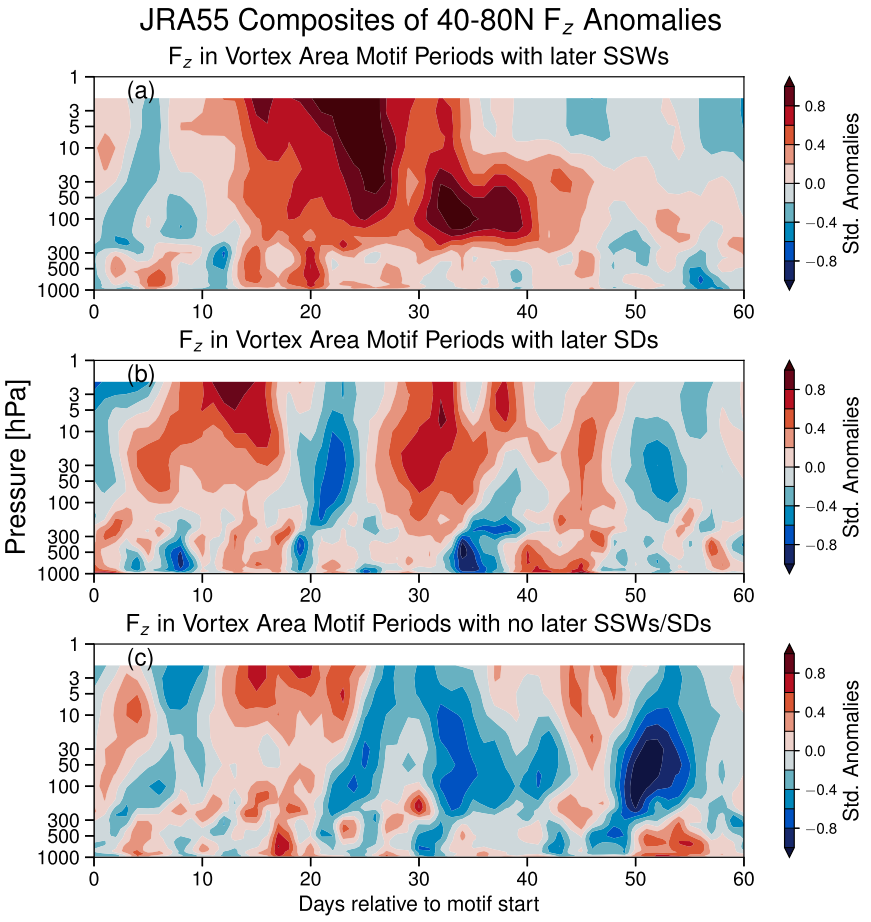

FIG. 10. Composites of standardized anomalies in the vertical component of EP-fluxes F_z averaged over 40°–80°N, composited using start dates from vortex area motifs with (a) later SSWs, (b) later significant disturbances (SDs), and (c) neither.

nearly split, or the zonal-mean zonal wind time series in their Figs. 2, 6, and 11 that still show deceleration to near reversals. In this sense, the perturbations to the stratospheric initial conditions in their experiments could be argued to have (in many of the cases) "lessened" the preconditioning rather than to have "turned it off."

5. Conclusions

We have used dynamic time warping (DTW) and a simple clustering algorithm to identify common stratospheric vortex characteristics, or motifs, prior to major sudden stratospheric warmings (SSWs) in reanalysis data. The motif composites paint a much clearer picture of vortex characteristics preceding SSWs than do simple composites relative to SSW central dates, particularly because of the reduced variability that comes about from the DTW optimally "aligning" the features in time. Previous studies have discussed specific signs that are thought to be representative of preconditioning of the vortex, including sharpened potential vorticity (PV) gradients in the vortex edge region (McIntyre 1982; McIntyre and Palmer 1984; Scott et al. 2004; Albers and Birner 2014; Liu and Scott 2015; Scott 2016; Jucker and Reichler 2018), reduced vortex area (McIntyre and Palmer 1983; Butchart and Remsberg 1986; Baldwin and Holton 1988), and changes to the strength of the polar night jet (McIntyre 1982; Albers and Birner 2014). We thus used data from CAVE-ART (Lawrence and Manney 2018) based on JRA-55 and MERRA-2, and specifically focused on diagnostics that would reflect these characteristics if they were apparent: vortex edge-averaged PV gradients, vortex area, and vortex edge-averaged wind speeds.

The 30-day pre-SSW motifs we found appear consistent with the aforementioned specific preconditioning signals in that the motif patterns showed a decrease in vortex area in the middle to upper stratosphere, an increase in PV gradients in the vortex edge region throughout the stratosphere, and a strengthening jet.

These motifs were apparent prior to about 75% of observed major SSWs; events that had no associated motifs primarily came from years with two SSWs (with one being ''captured'' and the other not) or those with early SSWs in late November or early December. We reiterate that the absence of motif patterns for these cases does not necessarily mean no relevant preconditioning patterns existed in such cases, only that the patterns were not similar enough based on our criterion to end up in the cluster of motifs considered here. We further examined the approximate lead times of these motif patterns relative to the central dates of SSWs and found that the median lead times for which the vortex area and vortex edge wind speed motifs are apparent in their entirety are approximately 8–10 days, while that for the vortex edge PV gradient motifs is approximately 23–24 days. Furthermore, vortex characteristics in cases with long leads greater than 20 days were largely persistent; that is, vortex area stayed reduced and PV gradients in the edge region remained enhanced until the SSWs occurred.

We also searched through years without SSWs using DTW to locate similar vortex characteristics, and found that similar motifs existed in over 90% of the remaining years. Approximately one-half (JRA-55 record) to two-thirds (MERRA-2 record) of these motifs appear in winters with significant disturbances that do not quite meet the threshold to classify as major SSWs. Including these significant disturbances to calculate the relative lead times of the motifs barely alters the statistics, and in fact brings JRA-55 and MERRA-2 closer to agreement, with median leads of approximately 25–26, 9–10, and 9 days, for edge-averaged PV gradients, edge-averaged wind speeds, and vortex area, respectively. Despite the large representation of motifs from years without major SSWs, there appears to be a strong association between the non-SSW motif signals and polar cap warming and zonal wind deceleration indicative of minor warmings confined primarily to the middle and upper stratosphere.

The results derived based on JRA-55 and MERRA-2 generally agree well, despite MERRA-2's shorter record. The most substantial differences between the two reanalyses are in the structure and magnitude of the vortex edge-averaged PV gradients as seen in the motif composites. These differences are systematic and likely due to a combination of factors: First, the PV fields from MERRA-2 are a provided model-level product, whereas we have derived those for JRA-55 using its model-level wind and temperature fields. A test case where we calculated vortex edge PV gradients using PV derived from MERRA-2 in the same manner as that for JRA-55 shows that the calculated gradients do tend to be systematically smaller than those calculated from the provided PV (not shown). Work for a separate paper is in progress that seeks to clarify how PV derived from model-level wind and temperature fields affects quantities derived from PV when compared to those derived from provided PV fields (and/or those derived from absolute/relative vorticity fields; L. Millán et al. 2020, unpublished manuscript). It has also been shown that reanalyses can have large differences in dynamical fields in the middle and upper stratosphere that may influence the vertical and horizontal structure of PV (Long et al. 2017). Finally, the calculations of PV gradients also depend on the horizontal (especially meridional) resolution of the gridded data, which differs between MERRA-2 and JRA-55. Regardless of the relative biases in the vortex edge-averaged PV gradients, the motif dates found in the 1980–2018 period were similar for both of the reanalyses. The vortex edge-averaged PV gradient anomaly composites also look very similar for both reanalyses, which indicates similar variability with respect to the reanalysis climatologies, and that the vortex edge PV gradient evolution shown is robust.

Our study has primarily made use of diagnostics from CAVE-ART, which are based on characteristics of the vortex proper regardless of its movement or geometrical state, unlike zonal-mean quantities. Furthermore, our results showed the evolution of such characteristics through most of the stratosphere rather than focusing on a single level in the middle stratosphere. It is possible that vertical variations in vortex characteristics are necessary to fully describe realistic evolution of the vortex toward SSWs. Methods and results like those described here could be used to evaluate whether models reproduce similar vortex characteristics prior to vortex disturbances. We did not seek to draw direct cause and effect relationships between the motifs and the generation of major sudden warmings or vortex disturbances, but rather to determine whether and when signs that have primarily been inferred as being indicative of preconditioning in observational and modeling studies were actually apparent in quantities that describe the state of the vortex. There is strong modeling evidence (e.g., from de la Cámara et al. 2017) that the stratospheric state is important in the development toward sudden warmings, but it would be interesting to perform similar modeling studies instead beginning with supposedly preconditioned initial conditions that do not lead to a major SSW, and evaluating whether and under what circumstances major warmings could be ''coaxed'' to occur.

Our focus on preconditioning is in part motivated by better understanding the prewarming development of SSWs. The motifs found here could potentially be useful in a predictive capacity, but given their large representation across years with and without major SSWs, they would

likely only provide insight in a probabilistic sense [e.g., similar to the work by Jucker and Reichler (2018)]. An advantage of dynamic time warping is that it does not require time series of equal lengths to work, so for example, dynamic time warping could be used to monitor near-real-time data or forecasts of differing lengths to, for example, find or sort nearest analogs among previous cases (such as the motifs found here). It would also be worthwhile to further explore whether there is a relationship between minor warming events and later larger vortex disturbances.

We also note that dynamic time warping could be useful for other geophysical problems. One aspect that we did not use herein is the "warping path" that dynamic time warping generates to minimize a given distance measure. These warping paths could be examined in detail to provide some general information about time scales and time lags separate from other techniques such as lagged correlations. Such information could be useful to identify or handle time-varying correlations.

Acknowledgments. We thank Ken Minschwaner and Krzysztof Wargan for helpful comments and discussion regarding this manuscript. We also thank the Microwave Limb Sounder team at the Jet Propulsion Laboratory, especially Brian Knosp and Luis Millán, for computational, data management, and data processing support. We are grateful to John Albers and two anonymous reviewers for comments that improved this manuscript. ZDL was funded by NASA Earth and Space Science Fellowship NNX16AO19H. ZDL and GLM were both supported under NASA Grant 80NSSC18K0053. GLM was also supported under a contract with the Microwave Limb Sounder project at JPL. JRA-55 data are publicly available from the NCAR Research Data Archive (at https://rda.ucar.edu/datasets/ds628.0/). MERRA-2 data are also publicly available from the NASA Data and Information Services Center (at https://disc.sci.gsfc.nasa.gov/uui/datasets?keywords=%22MERRA-2%22). The S-RIP zonal-mean datasets of dynamical variables are available from the Centre for Environmental Data Analysis (at https://catalogue.ceda.ac.uk/uuid/b241a7f536a244749662360bd7839312). Output from CAVE-ART as applied to these reanalyses can be provided upon request; please contact ZDL if you are interested in using the CAVE-ART products.

APPENDIX

Dynamic Time Warping

Let $X = (x_1, x_2, \ldots, x_i, \ldots, x_m)$ and $Y = (y_1, y_2, \ldots, y_j, \ldots, y_n)$ be sequences, and $W = (w_1, w_2, \ldots, w_k, \ldots, w_p)$ be a warping path that for each w_k maps to an index pairing $(i, j)_k$ of the sequences X and Y. Given a distance measure function $d(i, j)$, such as $d(i, j) = |x_i - y_j|$, the DTW procedure finds a warping path W^* such that the cumulative "distance" or cost is minimized; that is, $\mathrm{DTW}(X, Y) = \min\left[\sum d(W)\right] = \sum_{k=1}^{p} d(w_k^*)$. Clearly an exhaustive search through all possible warping paths would be computationally inefficient, and even if it were feasible, it could give potentially unrealistic and useless results (e.g., if a warping path is chosen such that all points in X are mapped to only one or two points in Y). Hence, certain constraints are typically imposed on the possible warping paths, which include: monotonicity (requiring that for all index pairs in the warping path $(i, j)_{k-1} \leq (i, j)_k$); continuity (requiring that "steps" along the warping path are confined to index neighbors; i.e., $i_k - i_{k-1} \leq 1$ and $j_k - j_{k-1} \leq 1$); boundary conditions (requiring that the first and last points in the warping path match a given condition, such as $(i, j)_1 = (1, 1)$ and $(i, j)_k = (m, n)$); slope constraints (requiring that the warping path in the $m \times n$ index space be restricted from being too steep or shallow); and window constraints (requiring that all points in the warping path are within a window of one another; i.e., $|i_k - j_k| \leq R$ for $R > 0$).

In practice, those wishing to use DTW need not implement the algorithms and constraints themselves, as DTW is implemented in scientific programming languages such as MATLAB and R, or provided in libraries and modules for general purpose languages such as Python (see, e.g., fastdtw).

REFERENCES

Albers, J. R., and T. Birner, 2014: Vortex preconditioning due to planetary and gravity waves prior to sudden stratospheric warmings. *J. Atmos. Sci.*, **71**, 4028–4054, https://doi.org/10.1175/JAS-D-14-0026.1.

Andrews, D. G., J. R. Holton, and C. B. Leovy, 1987: *Middle Atmosphere Dynamics*. International Geophysics Series, Vol. 40, Academic Press, 489 pp.

Attard, H. E., R. Rios-Berrios, C. T. Guastini, and A. L. Lang, 2016: Tropospheric and stratospheric precursors to the January 2013 sudden stratospheric warming. *Mon. Wea. Rev.*, **144**, 1321–1339, https://doi.org/10.1175/MWR-D-15-0175.1.

Baldwin, M. P., and J. R. Holton, 1988: Climatology of the stratospheric polar vortex and planetary wave breaking. *J. Atmos. Sci.*, **45**, 1123–1142, https://doi.org/10.1175/1520-0469(1988)045<1123:COTSPV>2.0.CO;2.

Bancalá, S., K. Krüger, and M. Giorgetta, 2012: The preconditioning of major sudden stratospheric warmings. *J. Geophys. Res.*, **117**, D04101, https://doi.org/10.1029/2011JD016769.

Berndt, D. J., and J. Clifford, 1994: Using dynamic time warping to find patterns in time series. *Proc. Third Int. Conf. on Knowledge Discovery and Data Mining*, Seattle, WA, Association for Computing Machinery, 359–370.

Birner, T., and J. R. Albers, 2017: Sudden stratospheric warmings and anomalous upward wave activity flux. *SOLA*, **13A**, 8–12, https://doi.org/10.2151/sola.13A-002.

Butchart, N., and E. E. Remsberg, 1986: The area of the stratospheric polar vortex as a diagnostic for tracer transport on an isentropic surface. *J. Atmos. Sci.*, **43**, 1319–1339, https://doi.org/10.1175/1520-0469(1986)043<1319:TAOTSP>2.0.CO;2.

——, S. A. Clough, T. N. Palmer, and P. J. Trevelyan, 1982: Simulations of an observed stratospheric warming with quasigeostrophic refractive index as a model diagnostic. *Quart. J. Roy. Meteor. Soc.*, **108**, 475–502, https://doi.org/10.1002/qj.49710845702.

Butler, A. H., L. M. Polvani, and C. Deser, 2014: Separating the stratospheric and tropospheric pathways of El Niño–Southern Oscillation teleconnections. *Environ. Res. Lett.*, **9**, 024014, https://doi.org/10.1088/1748-9326/9/2/024014.

——, D. J. Seidel, S. C. Hardiman, N. Butchart, T. Birner, and A. Match, 2015: Defining sudden stratospheric warmings. *Bull. Amer. Meteor. Soc.*, **96**, 1913–1928, https://doi.org/10.1175/BAMS-D-13-00173.1.

——, J. P. Sjoberg, D. J. Seidel, and K. H. Rosenlof, 2017: A sudden stratospheric warming compendium. *Earth Syst. Sci. Data*, **9**, 63–76, https://doi.org/10.5194/essd-9-63-2017.

Charlton, A. J., and L. M. Polvani, 2007: A new look at stratospheric sudden warmings. Part I: Climatology and modeling benchmarks. *J. Climate*, **20**, 449–469, https://doi.org/10.1175/JCLI3996.1.

Charlton-Perez, A. J., L. Ferranti, and R. W. Lee, 2018: The influence of the stratospheric state on North Atlantic weather regimes. *Quart. J. Roy. Meteor. Soc.*, **144**, 1140–1151, https://doi.org/10.1002/qj.3280.

Chen, P., and W. A. Robinson, 1992: Propagation of planetary waves between the troposphere and stratosphere. *J. Atmos. Sci.*, **49**, 2533–2545, https://doi.org/10.1175/1520-0469(1992)049<2533:POPWBT>2.0.CO;2.

Clark, J. H. E., 1974: Atmospheric response to the quasi-resonant growth of forced planetary waves. *J. Meteor. Soc. Japan*, **52**, 143–163, https://doi.org/10.2151/jmsj1965.52.1_143.

Cohen, J., and J. Jones, 2011: Tropospheric precursors and stratospheric warmings. *J. Climate*, **24**, 6562–6572, https://doi.org/10.1175/2011JCLI4160.1.

Colucci, S. J., and T. S. Ehrmann, 2018: Synoptic–dynamic climatology of the Aleutian high. *J. Atmos. Sci.*, **75**, 1271–1283, https://doi.org/10.1175/JAS-D-17-0215.1.

Coughlin, K., and L. J. Gray, 2009: A continuum of sudden stratospheric warmings. *J. Atmos. Sci.*, **66**, 531–540, https://doi.org/10.1175/2008JAS2792.1.

Coy, L., and S. Pawson, 2015: The major stratospheric sudden warming of January 2013: Analyses and forecasts in the GEOS-5 data assimilation system. *Mon. Wea. Rev.*, **143**, 491–510, https://doi.org/10.1175/MWR-D-14-00023.1.

——, S. Eckermann, and K. Hoppel, 2009: Planetary wave breaking and tropospheric forcing as seen in the stratospheric sudden warming of 2006. *J. Atmos. Sci.*, **66**, 495–507, https://doi.org/10.1175/2008JAS2784.1.

de la Cámara, A., J. R. Albers, T. Birner, R. R. Garcia, P. Hitchcock, D. E. Kinnison, and A. K. Smith, 2017: Sensitivity of sudden stratospheric warmings to previous stratospheric conditions. *J. Atmos. Sci.*, **74**, 2857–2877, https://doi.org/10.1175/JAS-D-17-0136.1.

——, T. Birner, and J. R. Albers, 2019: Are sudden stratospheric warmings preceded by anomalous tropospheric wave activity? *J. Climate*, **32**, 7173–7189, https://doi.org/10.1175/JCLI-D-19-0269.1.

Díaz-Durán, A., E. Serrano, B. Ayarzagüena, M. Abalos, and A. de la Cámara, 2017: Intra-seasonal variability of extreme boreal stratospheric polar vortex events and their precursors. *Climate Dyn.*, **49**, 3473–3491, https://doi.org/10.1007/s00382-017-3524-1.

Domeisen, D. I. V., A. H. Butler, K. Fröhlich, M. Bittner, W. A. Müller, and J. Baehr, 2015: Seasonal predictability over Europe arising from El Niño and stratospheric variability in the MPI-ESM seasonal prediction system. *J. Climate*, **28**, 256–271, https://doi.org/10.1175/JCLI-D-14-00207.1.

——, O. Martius, and B. Jiménez-Esteve, 2018: Rossby wave propagation into the Northern Hemisphere stratosphere: The role of zonal phase speed. *Geophys. Res. Lett.*, **45**, 2064–2071, https://doi.org/10.1002/2017GL076886.

Dunkerton, T. J., and D. P. Delisi, 1986: Evolution of potential vorticity in the winter stratosphere of January-February 1979. *J. Geophys. Res.*, **91**, 1199–1208, https://doi.org/10.1029/JD091iD01p01199.

Ebita, A., and Coauthors, 2011: The Japanese 55-year Reanalysis "JRA-55": An interim report. *SOLA*, **7**, 149–152, https://doi.org/10.2151/sola.2011-038.

Ern, M., and Coauthors, 2016: Satellite observations of middle atmosphere gravity wave absolute momentum flux and of its vertical gradient during recent stratospheric warmings. *Atmos. Chem. Phys.*, **16**, 9983–10 019, https://doi.org/10.5194/acp-16-9983-2016.

Esler, J. G., and N. J. Matthewman, 2011: Stratospheric sudden warmings as self-tuning resonances. Part II: Vortex displacement events. *J. Atmos. Sci.*, **68**, 2505–2523, https://doi.org/10.1175/JAS-D-11-08.1.

——, and M. Mester, 2019: Noise-induced vortex-splitting stratospheric sudden warmings. *Quart. J. Roy. Meteor. Soc.*, **145**, 476–494, https://doi.org/10.1002/qj.3443.

Fujiwara, M., and Coauthors, 2017: Introduction to the SPARC Reanalysis Intercomparison Project (S-RIP) and overview of the reanalysis systems. *Atmos. Chem. Phys.*, **17**, 1417–1452, https://doi.org/10.5194/acp-17-1417-2017.

Gelaro, R., and Coauthors, 2017: The Modern-Era Retrospective analysis for Research and Applications, version 2 (MERRA-2). *J. Climate*, **30**, 5419–5454, https://doi.org/10.1175/JCLI-D-16-0758.1.

Gerber, E. P., and L. M. Polvani, 2009: Stratosphere–troposphere coupling in a relatively simple AGCM: The importance of stratospheric variability. *J. Climate*, **22**, 1920–1933, https://doi.org/10.1175/2008JCLI2548.1.

Hansen, F., T. Kruschke, R. J. Greatbatch, and A. Weisheimer, 2019: Factors influencing the seasonal predictability of Northern Hemisphere severe winter storms. *Geophys. Res. Lett.*, **46**, 365–373, https://doi.org/10.1029/2018GL079415.

Hitchcock, P., and P. H. Haynes, 2016: Stratospheric control of planetary waves. *Geophys. Res. Lett.*, **43**, 11 884–11 892, https://doi.org/10.1002/2016GL071372.

Hu, J., R. Ren, and H. Xu, 2014: Occurrence of winter stratospheric sudden warming events and the seasonal timing of spring stratospheric final warming. *J. Atmos. Sci.*, **71**, 2319–2334, https://doi.org/10.1175/JAS-D-13-0349.1.

Huang, J., W. Tian, L. J. Gray, J. Zhang, Y. Li, J. Luo, and H. Tian, 2018: Preconditioning of Arctic stratospheric polar vortex shift events. *J. Climate*, **31**, 5417–5436, https://doi.org/10.1175/JCLI-D-17-0695.1.

Itakura, F., 1975: Minimum prediction residual principle applied to speech recognition. *IEEE Trans. Acoust. Speech Signal Process.*, **23**, 67–72, https://doi.org/10.1109/TASSP.1975.1162641.

Jucker, M., 2016: Are sudden stratospheric warmings generic? Insights from an idealized GCM. *J. Atmos. Sci.*, **73**, 5061–5080, https://doi.org/10.1175/JAS-D-15-0353.1.

——, and T. Reichler, 2018: Dynamical precursors for statistical prediction of stratospheric sudden warming events. *Geophys. Res. Lett.*, **45**, 13 124–13 132, https://doi.org/10.1029/2018GL080691.

Kanzawa, H., 1980: The behavior of mean zonal wind and planetary-scale disturbances in the troposphere and stratosphere during the 1973 sudden warming. *J. Meteor. Soc. Japan*, **58**, 329–356, https://doi.org/10.2151/jmsj1965.58.5_329.

Karpechko, A. Y., 2018: Predictability of sudden stratospheric warmings in the ECMWF extended-range forecast system. *Mon. Wea. Rev.*, **146**, 1063–1075, https://doi.org/10.1175/MWR-D-17-0317.1.

——, P. Hitchcock, D. H. W. Peters, and A. Schneidereit, 2017: Predictability of downward propagation of major sudden stratospheric warmings. *Quart. J. Roy. Meteor. Soc.*, **143**, 1459–1470, https://doi.org/10.1002/qj.3017.

——, A. Charlton-Perez, M. Balmaseda, N. Tyrrell, and F. Vitart, 2018: Predicting sudden stratospheric warming 2018 and its climate impacts with a multimodel ensemble. *Geophys. Res. Lett.*, **45**, 13 538–13 546, https://doi.org/10.1029/2018GL081091.

Kidston, J., A. A. Scaife, S. C. Hardiman, D. M. Mitchell, N. Butchart, M. P. Baldwin, and L. J. Gray, 2015: Stratospheric influence on tropospheric jet streams, storm tracks and surface weather. *Nat. Geosci.*, **8**, 433–440, https://doi.org/10.1038/ngeo2424.

Kobayashi, S., and Coauthors, 2015: The JRA-55 reanalysis: General specification and basic characteristics. *J. Meteor. Soc. Japan*, **93**, 5–48, https://doi.org/10.2151/jmsj.2015-001.

Kretschmer, M., J. Runge, and D. Coumou, 2017: Early prediction of extreme stratospheric polar vortex states based on causal precursors. *Geophys. Res. Lett.*, **44**, 8592–8600, https://doi.org/10.1002/2017GL074696.

Kwasniok, F., R. Beaumont, and J. Thuburn, 2019: Vortex dynamics of stratospheric sudden warmings: A reanalysis data study using PV contour integral diagnostics. *Quart. J. Roy. Meteor. Soc.*, **145**, 1013–1033, https://doi.org/10.1002/qj.3474.

Labitzke, K., 1981: The amplification of height wave 1 in January 1979: A characteristic precondition for the major warming in February. *Mon. Wea. Rev.*, **109**, 983–989, https://doi.org/10.1175/1520-0493(1981)109<0983:TAOHWI>2.0.CO;2.

Lawrence, Z. D., and G. L. Manney, 2018: Characterizing stratospheric polar vortex variability with computer vision techniques. *J. Geophys. Res. Atmos.*, **123**, 1510–1535, https://doi.org/10.1002/2017JD027556.

Limpasuvan, V., D. W. J. Thompson, and D. L. Hartmann, 2004: The life cycle of the Northern Hemisphere sudden stratospheric warmings. *J. Climate*, **17**, 2584–2596, https://doi.org/10.1175/1520-0442(2004)017<2584:TLCOTN>2.0.CO;2.

Lin, B.-D., 1982: The behavior of winter stationary planetary waves forced by topography and diabatic heating. *J. Atmos. Sci.*, **39**, 1206–1226, https://doi.org/10.1175/1520-0469(1982)039<1206:TBOWSP>2.0.CO;2.

Lindgren, E. A., A. Sheshadri, and R. A. Plumb, 2018: Sudden stratospheric warming formation in an idealized general circulation model using three types of tropospheric forcing. *J. Geophys. Res. Atmos.*, **123**, 10 125–10 139, https://doi.org/10.1029/2018JD028537.

Liu, Y. S., and R. K. Scott, 2015: The onset of the barotropic sudden warming in a global model. *Quart. J. Roy. Meteor. Soc.*, **141**, 2944–2955, https://doi.org/10.1002/qj.2580.

Long, C. S., M. Fujiwara, S. Davis, D. M. Mitchell, and C. J. Wright, 2017: Climatology and interannual variability of dynamic variables in multiple reanalyses evaluated by the SPARC Reanalysis Intercomparison Project (S-RIP). *Atmos. Chem. Phys.*, **17**, 14 593–14 629, https://doi.org/10.5194/acp-17-14593-2017.

Manney, G. L., and Z. D. Lawrence, 2016: The major stratospheric final warming in 2016: Dispersal of vortex air and termination of Arctic chemical ozone loss. *Atmos. Chem. Phys.*, **16**, 15 371–15 396, https://doi.org/10.5194/acp-16-15371-2016.

——, M. L. Santee, L. Froidevaux, K. Hoppel, N. J. Livesey, and J. W. Waters, 2006: EOS MLS observations of ozone loss in the 2004-2005 Arctic winter. *Geophys. Res. Lett.*, **33**, L04802, https://doi.org/10.1029/2005GL024494.

Martineau, P., G. Chen, S.-W. Son, and J. Kim, 2018a: Lower-stratospheric control of the frequency of sudden stratospheric warming events. *J. Geophys. Res. Atmos.*, **123**, 3051–3070, https://doi.org/10.1002/2017JD027648.

——, J. S. Wright, N. Zhu, and M. Fujiwara, 2018b: Zonal-mean data set of global atmospheric reanalyses on pressure levels. *Earth Syst. Sci. Data*, **10**, 1925–1941, https://doi.org/10.5194/essd-10-1925-2018.

Martius, O., L. M. Polvani, and H. C. Davies, 2009: Blocking precursors to stratospheric sudden warming events. *Geophys. Res. Lett.*, **36**, L14806, https://doi.org/10.1029/2009GL038776.

Matsuno, T., 1971: A dynamical model of the stratospheric sudden warming. *J. Atmos. Sci.*, **28**, 1479–1494, https://doi.org/10.1175/1520-0469(1971)028<1479:ADMOTS>2.0.CO;2.

Matthewman, N. J., and J. G. Esler, 2011: Stratospheric sudden warmings as self-tuning resonances. Part I: Vortex splitting events. *J. Atmos. Sci.*, **68**, 2481–2504, https://doi.org/10.1175/JAS-D-11-07.1.

Maury, P., C. Claud, E. Manzini, A. Hauchecorne, and P. Keckhut, 2016: Characteristics of stratospheric warming events during northern winter. *J. Geophys. Res. Atmos.*, **121**, 5368–5380, https://doi.org/10.1002/2015JD024226.

McIntyre, M. E., 1982: How well do we understand the dynamics of stratospheric warmings? *J. Meteor. Soc. Japan*, **60**, 37–65, https://doi.org/10.2151/jmsj1965.60.1_37.

——, and T. N. Palmer, 1983: Breaking planetary waves in the stratosphere. *Nature*, **305**, 593–600, https://doi.org/10.1038/305593a0.

——, and ——, 1984: The ''surf zone'' in the stratosphere. *J. Atmos. Terr. Phys.*, **46**, 825–849, https://doi.org/10.1016/0021-9169(84)90063-1.

Mueen, A., E. Keogh, Q. Zhu, S. Cash, and B. Westover, 2009: Exact discovery of time series motifs. *Ninth Int. Conf. on Data Mining*, Sparks, NV, Society for Industrial and Applied Mathematics, 473–484, https://doi.org/10.1137/1.9781611972795.41.

Mukougawa, H., H. Sakai, and T. Hirooka, 2005: High sensitivity to the initial condition for the prediction of stratospheric sudden warming. *Geophys. Res. Lett.*, **32**, L17806, https://doi.org/10.1029/2005GL022909.

Nash, E. R., P. A. Newman, J. E. Rosenfield, and M. R. Schoeberl, 1996: An objective determination of the polar vortex using Ertel's potential vorticity. *J. Geophys. Res.*, **101**, 9471–9478, https://doi.org/10.1029/96JD00066.

Newman, P. A., and J. E. Rosenfield, 1997: Stratospheric thermal damping times. *Geophys. Res. Lett.*, **24**, 433–436, https://doi.org/10.1029/96GL03720.

Nishii, K., and H. Nakamura, 2010: Three-dimensional evolution of ensemble forecast spread during the onset of a stratospheric sudden warming event in January 2006. *Quart. J. Roy. Meteor. Soc.*, **136**, 894–905, https://doi.org/10.1002/qj.607.

Noguchi, S., H. Mukougawa, Y. Kuroda, R. Mizuta, S. Yabu, and H. Yoshimura, 2016: Predictability of the stratospheric polar vortex breakdown: An ensemble reforecast experiment for the splitting event in January 2009. *J. Geophys. Res. Atmos.*, **121**, 3388–3404, https://doi.org/10.1002/2015JD024581.

O'Neill, A., and C. E. Youngblut, 1982: Stratospheric warmings diagnosed using the transformed Eulerian-mean equations and the effect of the mean state on wave propagation. *J. Atmos. Sci.*, **39**, 1370–1386, https://doi.org/10.1175/1520-0469(1982)039<1370:SWDUTT>2.0.CO;2.

——, and V. D. Pope, 1988: Simulations of linear and nonlinear disturbances in the stratosphere. *Quart. J. Roy. Meteor. Soc.*, **114**, 1063–1110, https://doi.org/10.1002/qj.49711448210.

——, C. L. Oatley, A. J. Charlton-Perez, D. M. Mitchell, and T. Jung, 2017: Vortex splitting on a planetary scale in the stratosphere by cyclogenesis on a subplanetary scale in the troposphere. *Quart. J. Roy. Meteor. Soc.*, **143**, 691–705, https://doi.org/10.1002/qj.2957.

Palmeiro, F. M., D. Barriopedro, R. García-Herrera, and N. Calvo, 2015: Comparing sudden stratospheric warming definitions in reanalysis data. *J. Climate*, **28**, 6823–6840, https://doi.org/10.1175/JCLI-D-15-0004.1.

Palmer, T. N., 1981: Aspects of stratospheric sudden warmings studied from a transformed Eulerian-mean viewpoint. *J. Geophys. Res.*, **86**, 9679–9687, https://doi.org/10.1029/JC086iC10p09679.

——, and C.-P. F. Hsu, 1983: Stratospheric sudden coolings and the role of nonlinear wave interactions in preconditioning the circumpolar flow. *J. Atmos. Sci.*, **40**, 909–928, https://doi.org/10.1175/1520-0469(1983)040<0909:SSCATR>2.0.CO;2.

Plougonven, R., V. Jewtoukoff, A. Cámara, F. Lott, and A. Hertzog, 2017: On the relation between gravity waves and wind speed in the lower stratosphere over the Southern Ocean. *J. Atmos. Sci.*, **74**, 1075–1093, https://doi.org/10.1175/JAS-D-16-0096.1.

Plumb, R. A., 1981: Instability of the distorted polar night vortex: A theory of stratospheric warmings. *J. Atmos. Sci.*, **38**, 2514–2531, https://doi.org/10.1175/1520-0469(1981)038<2514:IOTDPN>2.0.CO;2.

Rao, J., R. Ren, H. Chen, Y. Yu, and Y. Zhou, 2018: The stratospheric sudden warming event in February 2018 and its prediction by a climate system model. *J. Geophys. Res. Atmos.*, **123**, 13 332–13 345, https://doi.org/10.1029/2018JD028908.

Reddy, D. R., 1976: Speech recognition by machine: A review. *Proc. IEEE*, **64**, 501–531, https://doi.org/10.1109/PROC.1976.10158.

Robinson, W. A., 1986: The behavior of planetary wave 2 in preconditioned zonal flows. *J. Atmos. Sci.*, **43**, 3109–3121, https://doi.org/10.1175/1520-0469(1986)043<3109:TBOPWI>2.0.CO;2.

Sakoe, H., and S. Chiba, 1978: Dynamic programming algorithm optimization for spoken word recognition. *IEEE Trans. Acoust. Speech Signal Process.*, **26**, 43–49, https://doi.org/10.1109/TASSP.1978.1163055.

Scaife, A. A., and Coauthors, 2016: Seasonal winter forecasts and the stratosphere. *Atmos. Sci. Lett.*, **17**, 51–56, https://doi.org/10.1002/asl.598.

Scott, R. K., 2016: A new class of vacillations of the stratospheric polar vortex. *Quart. J. Roy. Meteor. Soc.*, **142**, 1948–1957, https://doi.org/10.1002/qj.2788.

——, and L. M. Polvani, 2006: Internal variability of the winter stratosphere. Part I: Time-independent forcing. *J. Atmos. Sci.*, **63**, 2758–2776, https://doi.org/10.1175/JAS3797.1.

——, D. G. Dritschel, L. M. Polvani, and D. W. Waugh, 2004: Enhancement of Rossby wave breaking by steep potential vorticity gradients in the winter stratosphere. *J. Atmos. Sci.*, **61**, 904–918, https://doi.org/10.1175/1520-0469(2004)061<0904:EORWBB>2.0.CO;2.

Sheshadri, A., R. A. Plumb, and E. P. Gerber, 2015: Seasonal variability of the polar stratospheric vortex in an idealized AGCM with varying tropospheric wave forcing. *J. Atmos. Sci.*, **72**, 2248–2266, https://doi.org/10.1175/JAS-D-14-0191.1.

Shokoohi-Yekta, M., B. Hu, H. Jin, J. Wang, and E. Keogh, 2017: Generalizing DTW to the multi-dimensional case requires an adaptive approach. *Data Min. Knowl. Discovery*, **31**, 1–31, https://doi.org/10.1007/s10618-016-0455-0.

Sigmond, M., J. Scinocca, V. Kharin, and T. Shepherd, 2013: Enhanced seasonal forecast skill following stratospheric sudden warmings. *Nat. Geosci.*, **6**, 98–102, https://doi.org/10.1038/ngeo1698.

Sjoberg, J. P., and T. Birner, 2014: Stratospheric wave–mean flow feedbacks and sudden stratospheric warmings in a simple model forced by upward wave activity flux. *J. Atmos. Sci.*, **71**, 4055–4071, https://doi.org/10.1175/JAS-D-14-0113.1.

Smith, A. K., 1992: Preconditioning for stratospheric sudden warmings: Sensitivity studies with a numerical model. *J. Atmos. Sci.*, **49**, 1003–1019, https://doi.org/10.1175/1520-0469(1992)049<1003:PFSSWS>2.0.CO;2.

Smith, K. L., L. M. Polvani, and L. B. Tremblay, 2018: The impact of stratospheric circulation extremes on minimum Arctic sea ice extent. *J. Climate*, **31**, 7169–7183, https://doi.org/10.1175/JCLI-D-17-0495.1.

Sun, L., W. A. Robinson, and G. Chen, 2012: The predictability of stratospheric warming events: More from the troposphere or the stratosphere? *J. Atmos. Sci.*, **69**, 768–783, https://doi.org/10.1175/JAS-D-11-0144.1.

Taguchi, M., 2016: Connection of predictability of major stratospheric sudden warmings to polar vortex geometry. *Atmos. Sci. Lett.*, **17**, 33–38, https://doi.org/10.1002/asl.595.

——, 2018: Comparison of subseasonal-to-seasonal model forecasts for major stratospheric sudden warmings. *J. Geophys. Res. Atmos.*, **123**, 10 231–10 247, https://doi.org/10.1029/2018JD028755.

Tripathi, O. P., and Coauthors, 2015: The predictability of the extratropical stratosphere on monthly time-scales and its impact on the skill of tropospheric forecasts. *Quart. J. Roy. Meteor. Soc.*, **141**, 987–1003, https://doi.org/10.1002/qj.2432.

——, and Coauthors, 2016: Examining the predictability of the stratospheric sudden warming of January 2013 using multiple NWP systems. *Mon. Wea. Rev.*, **144**, 1935–1960, https://doi.org/10.1175/MWR-D-15-0010.1.

Tung, K. K., and R. S. Lindzen, 1979: A theory of stationary long waves. Part II: Resonant Rossby waves in the presence of realistic vertical shears. *Mon. Wea. Rev.*, **107**, 735–750, https://doi.org/10.1175/1520-0493(1979)107<0735:ATOSLW>2.0.CO;2.

Verleysen, M., and D. François, 2005: The curse of dimensionality in data mining and time series prediction. *Computational Intelligence and Bioinspired Systems*, J. Cabestany, A. Prieto, and F. Sandoval, Eds., Springer, 758–770.

Wang, L., and M. J. Alexander, 2009: Gravity wave activity during stratospheric sudden warmings in the 2007–2008 Northern Hemisphere winter. *J. Geophys. Res.*, **114**, D18108, https://doi.org/10.1029/2009JD011867.

White, G., and R. Neely, 1976: Speech recognition experiments with linear predication, bandpass filtering, and dynamic programming. *IEEE Trans. Acoust. Speech Signal Process.*, **24**, 183–188, https://doi.org/10.1109/TASSP.1976.1162779.

White, R. H., D. S. Battisti, and A. Sheshadri, 2018: Orography and the boreal winter stratosphere: The importance of the Mongolian mountains. *Geophys. Res. Lett.*, **45**, 2088–2096, https://doi.org/10.1002/2018GL077098.